Mid-Infrared Quantum Cascade Lasers

Claire Gmachl

Director of MIRTHE (NSF-ERC)

Eugene Higgins Professor of Electrical Engineering Princeton University

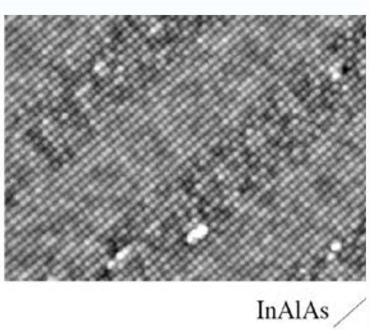

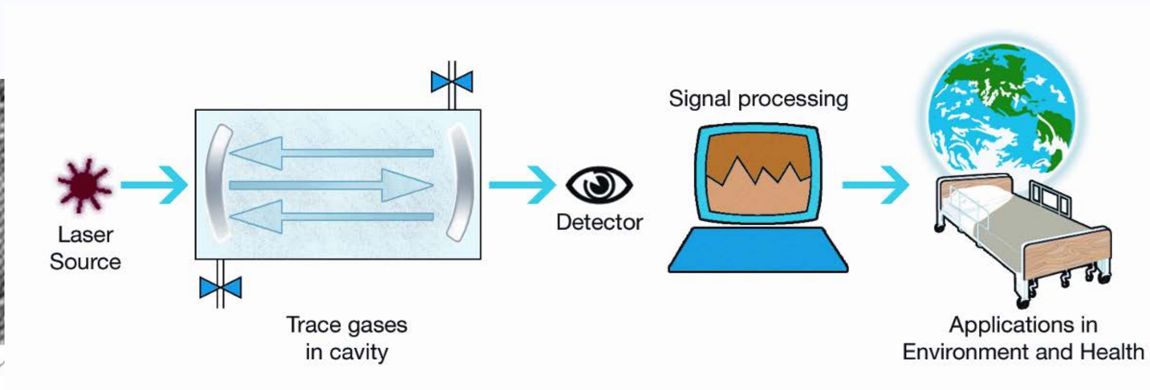

Summer 2012

Mid-Infrared Spectrum
And a Case for QC lasers

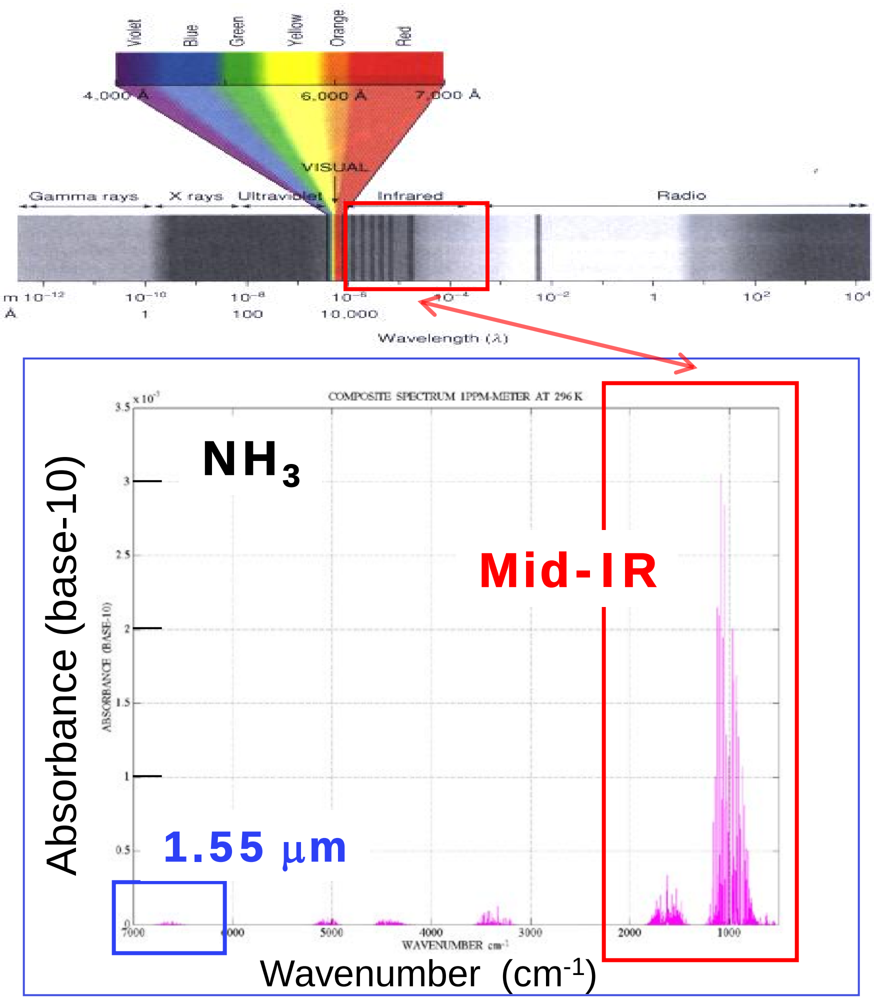

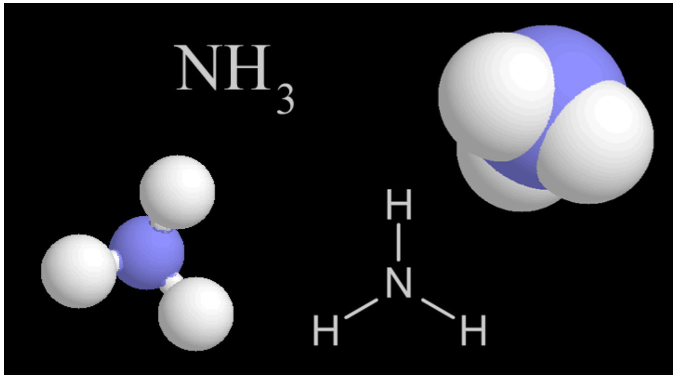

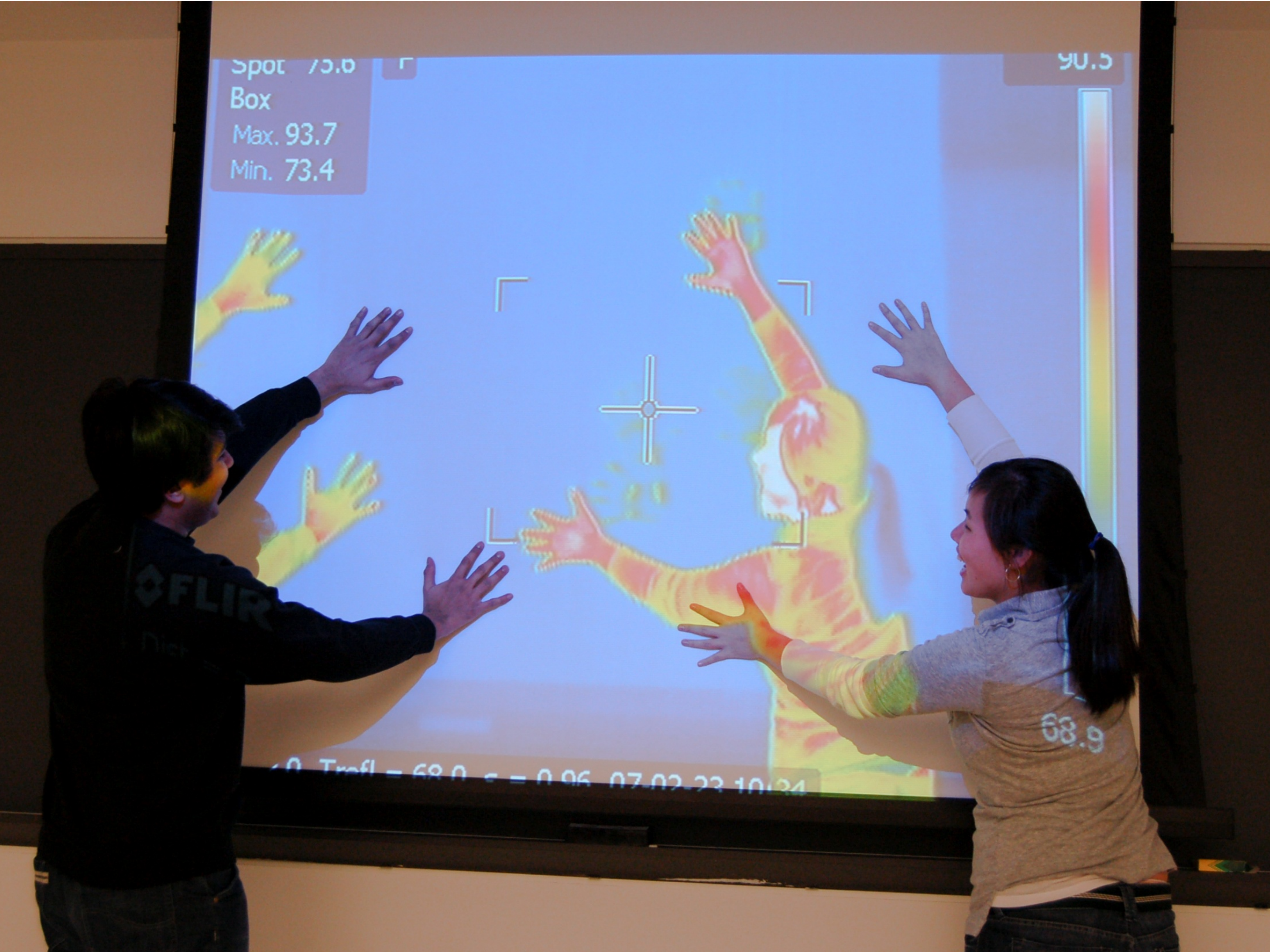
Box
Max. 93.7
Min. 73.4
68.9
FLIR

Quantum Cascade (QC) Laser

"Designer Material"
"Designer Laser"

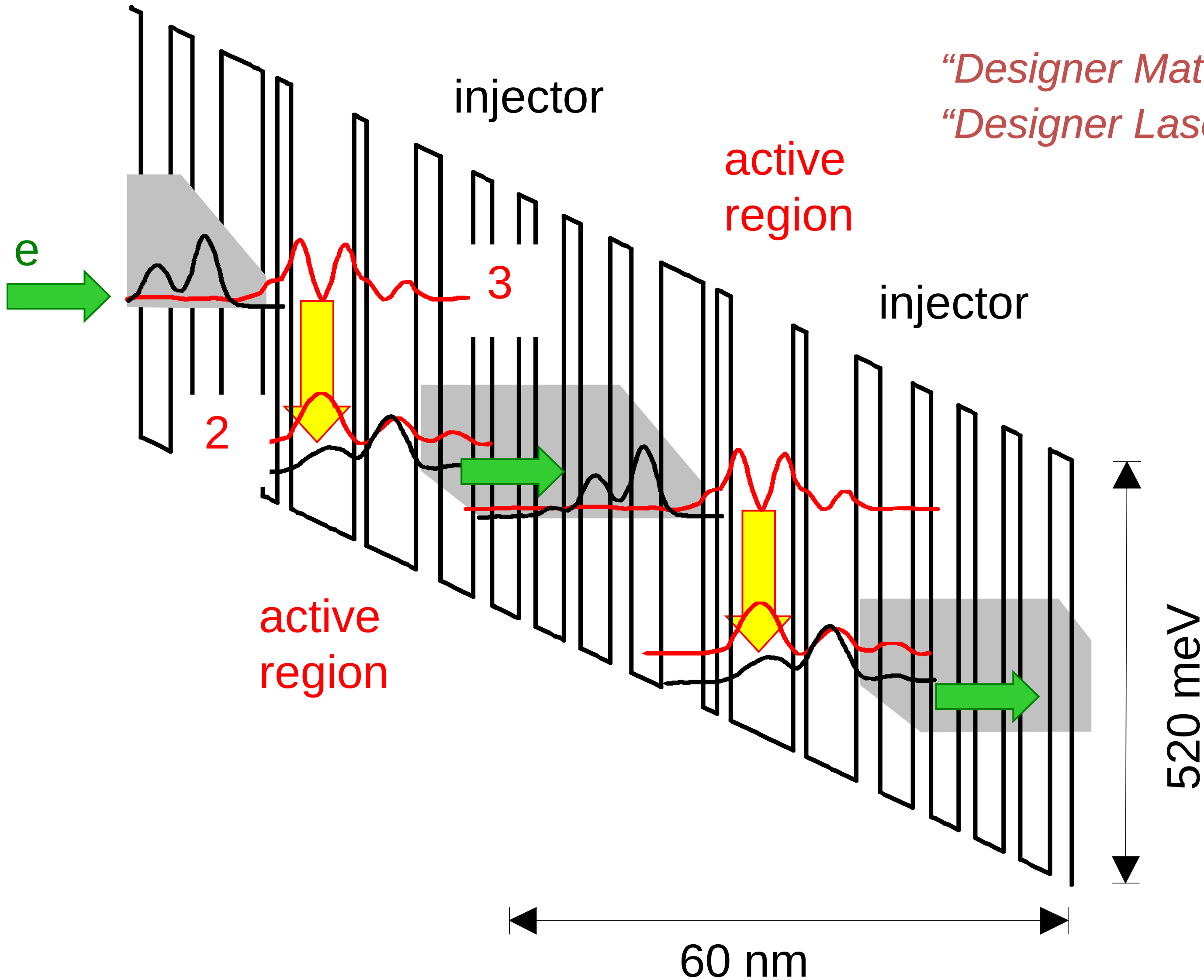

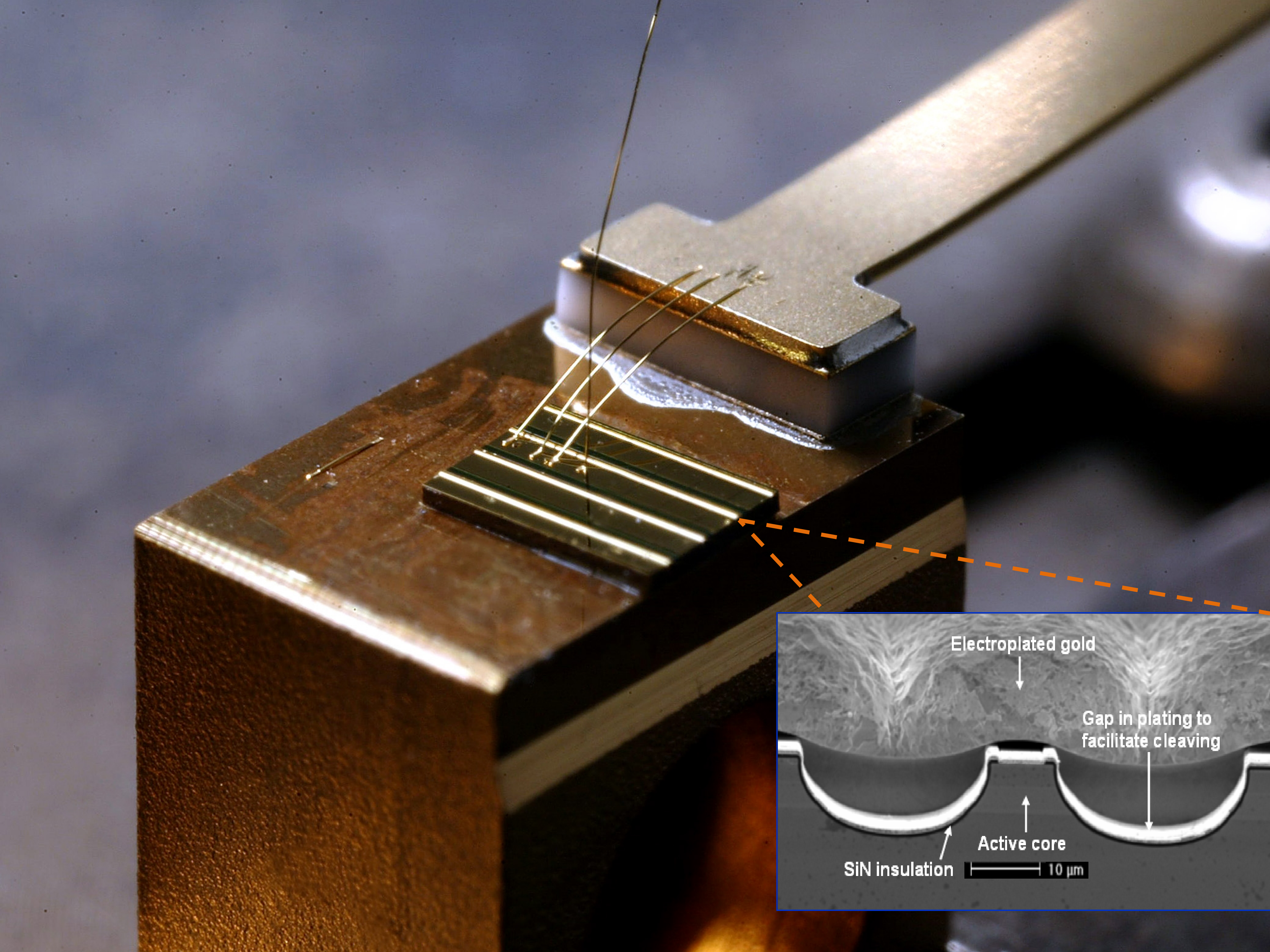
Electroplated gold
Gap in plating to facilitate cleaving
Active core
SiN insulation
10 µm

QC-Laser: Built Atom by Atom

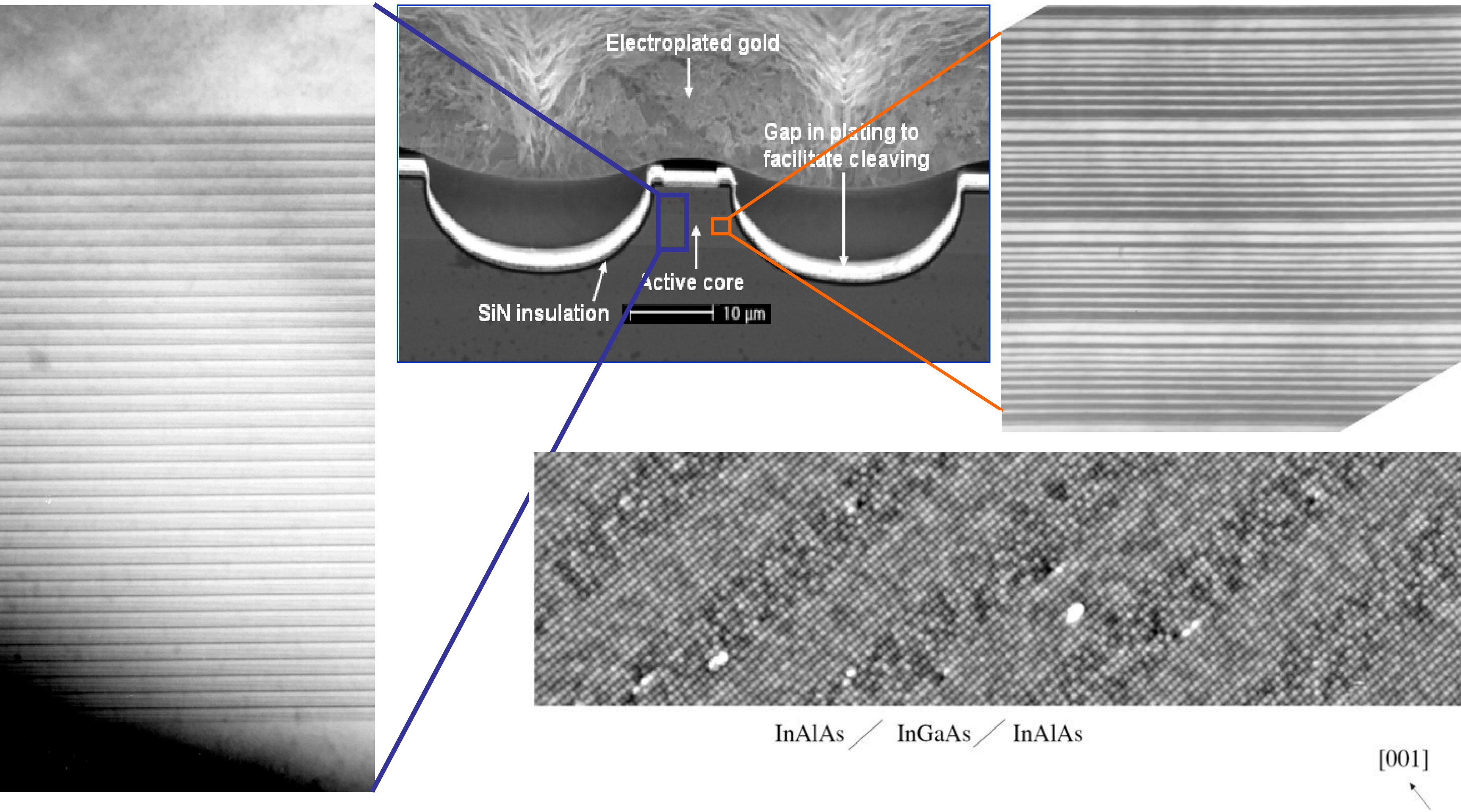

M. Weimer, TAMU

QC Laser @ λ ~ 4.7 μm

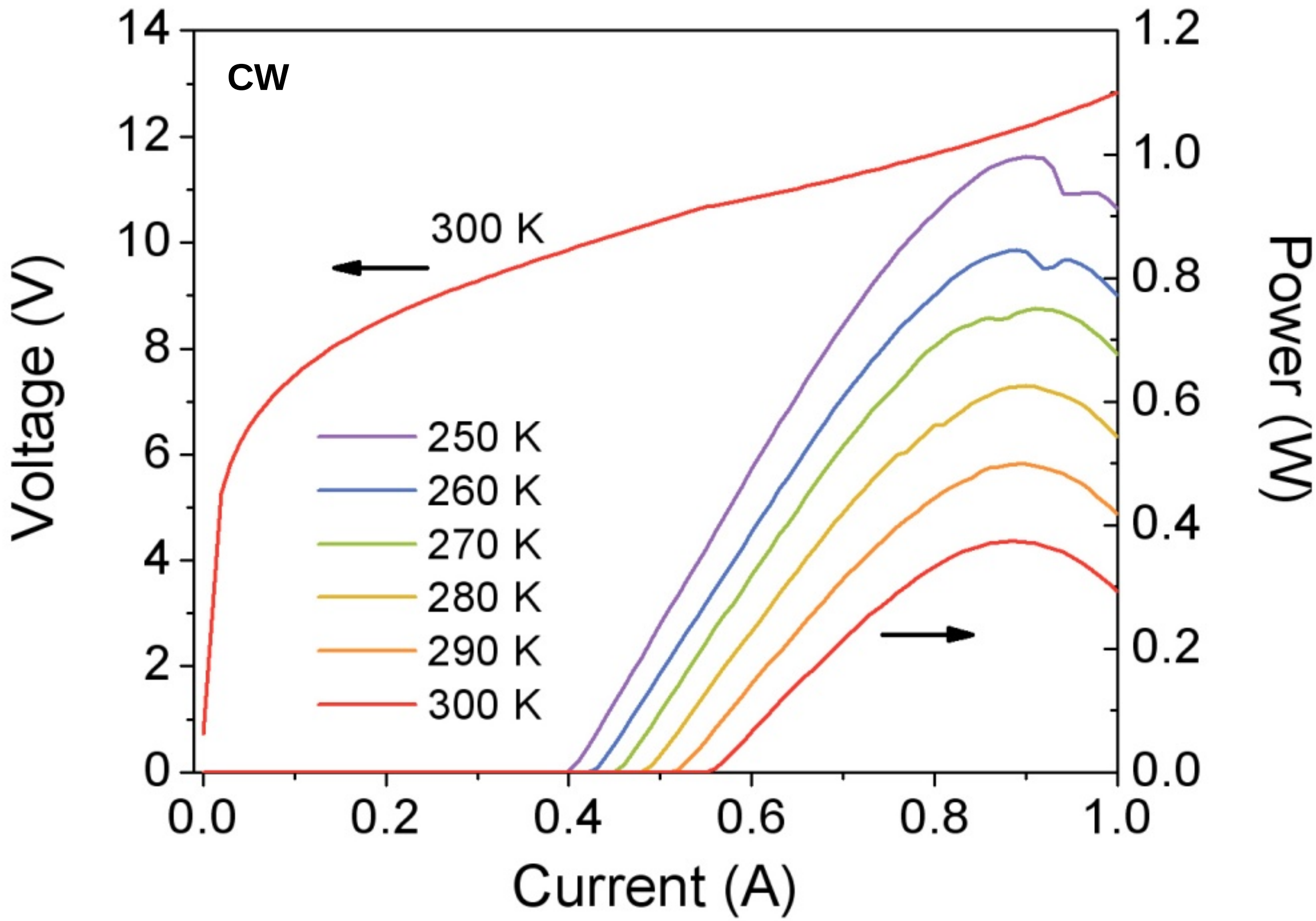

What Makes the QC-laser Special:

- Wavelength agility
  - layer thicknesses determine emission wavelength
  - InGaAs/AlInAs: 3 – 24 μm wavelength; -Sb < 3 μm
  - GaAs/AlGaAs: THz, 65 – ~ 300 μm wavelength
- Demonstrated applications in mid-IR gas sensing
- High optical power
  - cascading re-uses electrons
- Ultra-fast carrier dynamics
- Pure TM-polarization – efficient in-plane light coupling
- Small linewidth enhancement factor
- Intrinsic design potential; large *fun* factor

New directions in quantum design

Quest for high performance QC lasers

Peter Q. Liu, Yu Yao et al.
YenTing Chiu et al.

Theory:
Jacob Khurgin, Yamac Dikmelik, JHU

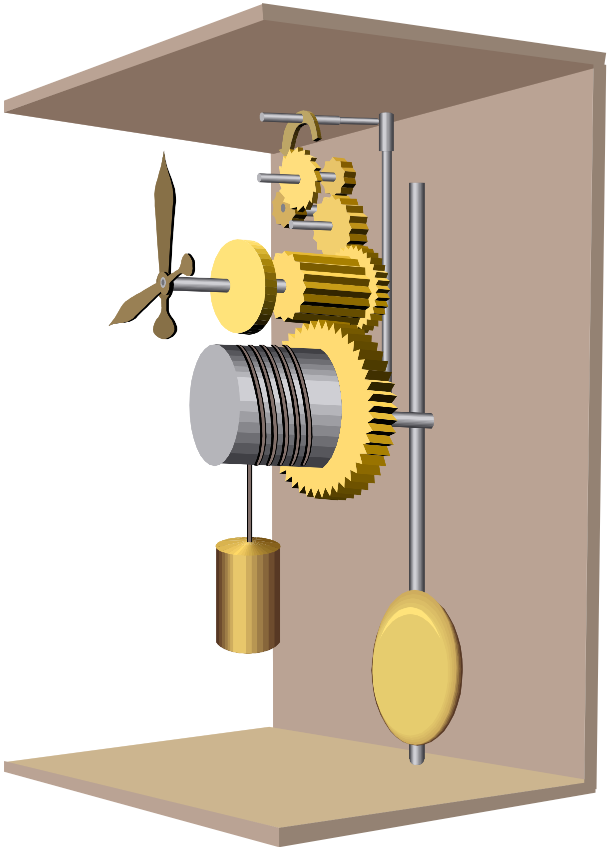

Interface Roughness in QC lasers

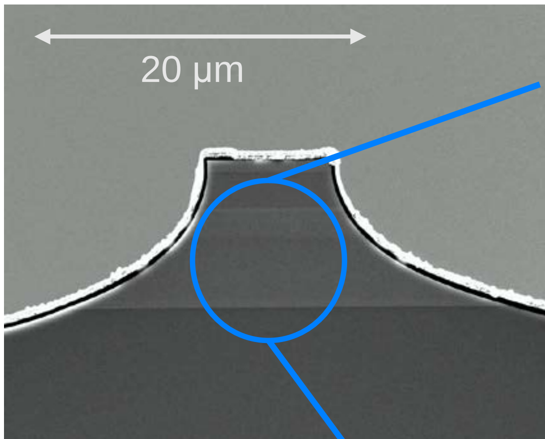

SEM

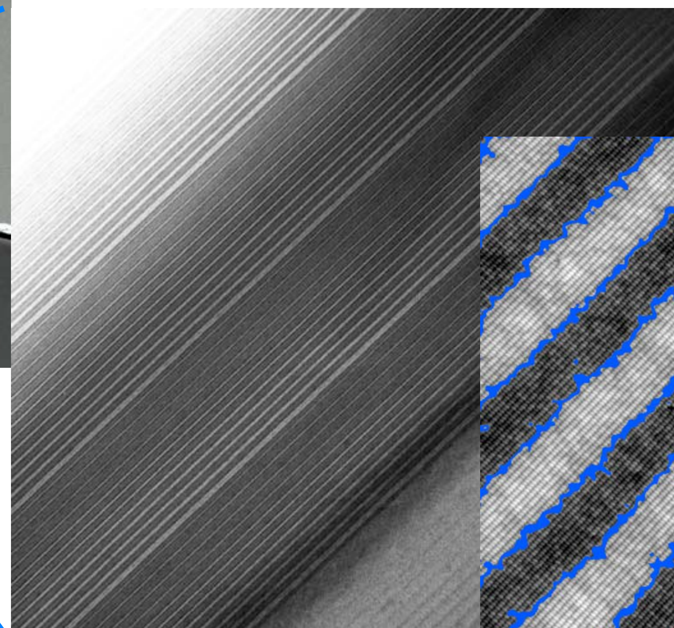

TEM
Courtesy of Dr. Nan Yao, Princeton University.

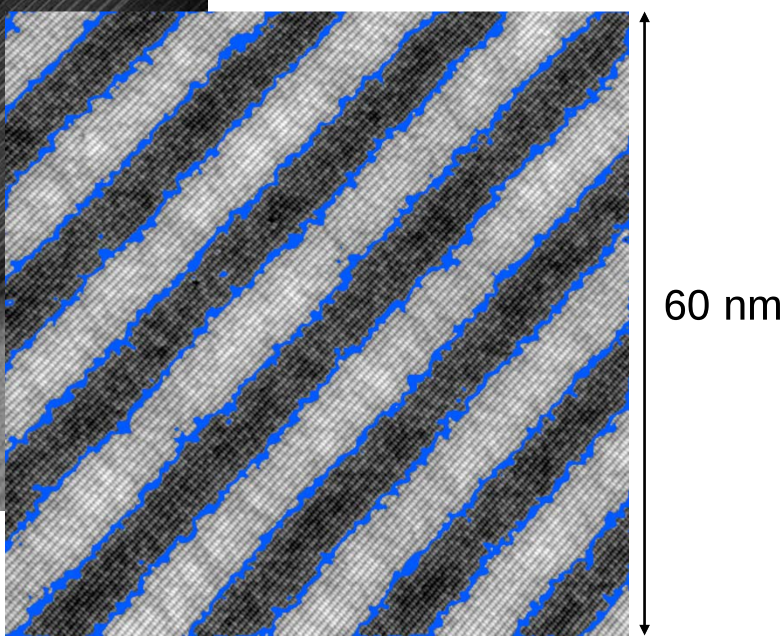

STM image of a superlattice structure.
Courtesy of Mathew Woods, Federico Lopez, Kara Kanedy and Michael Weimer, Texas A&M University.

Electron Transport: Resonant Tunneling

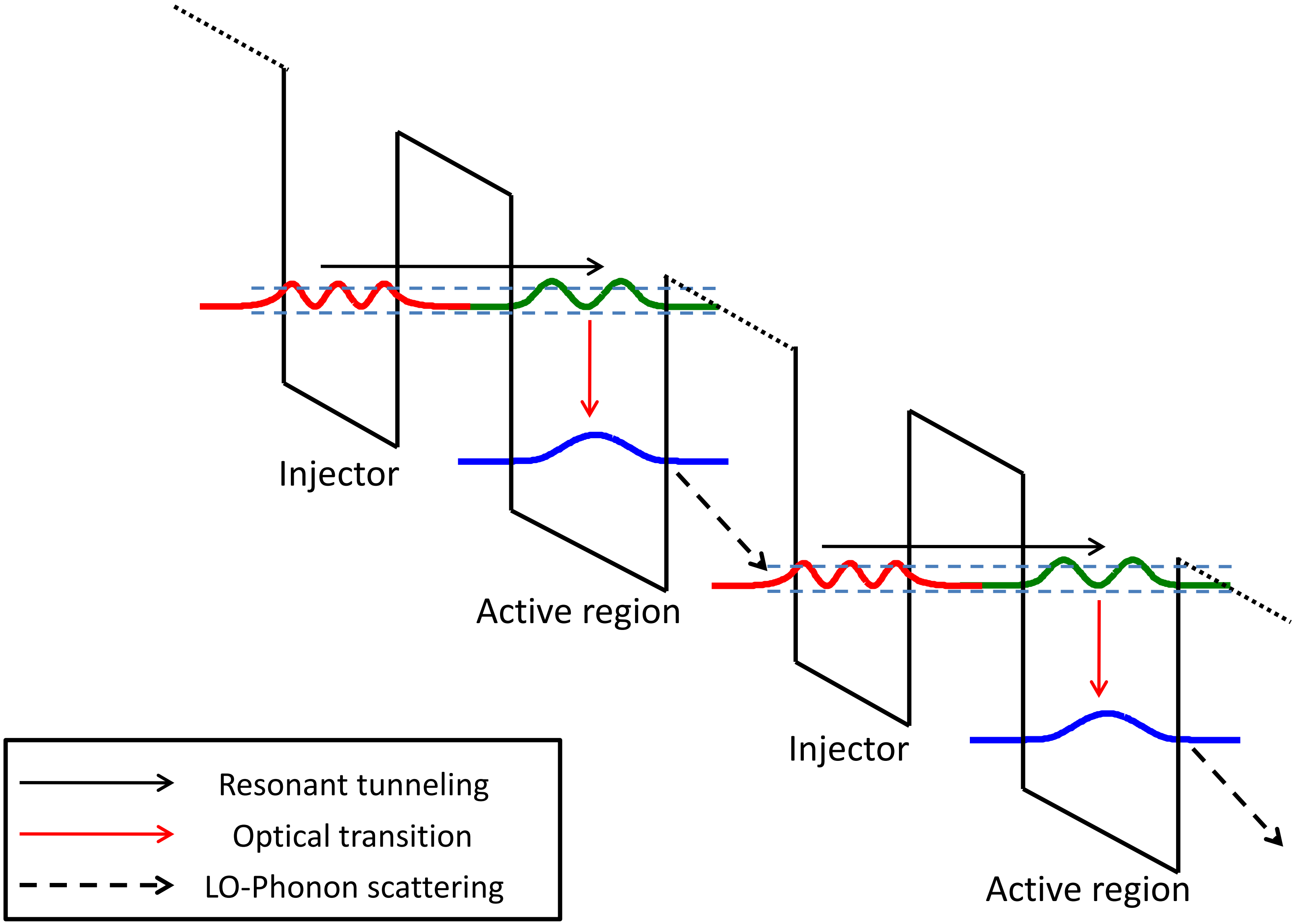

Interface Roughness & Tunneling

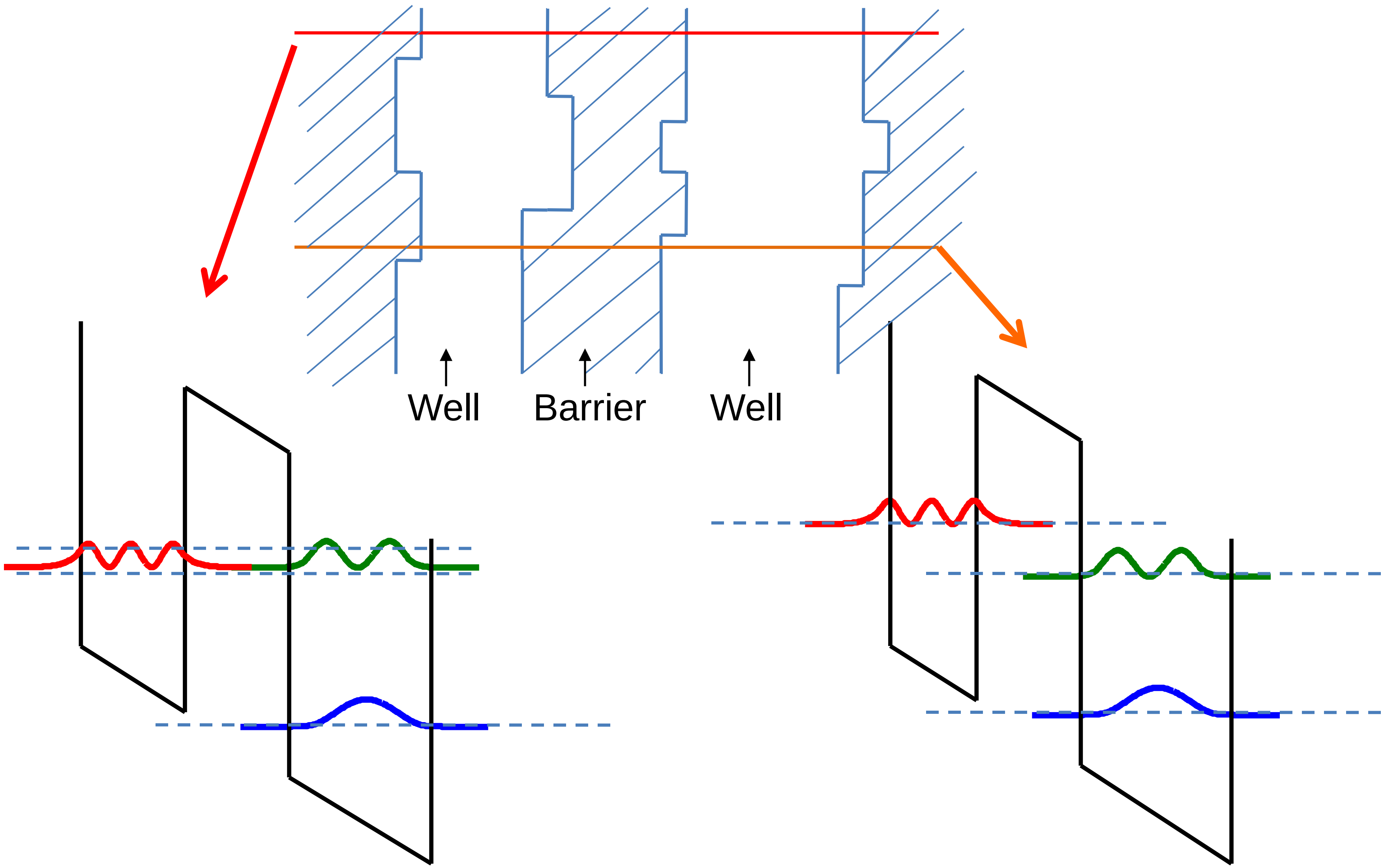

Modeling Interface Roughness Scattering

➢ Interface roughness also causes intersubband scattering!

Random perturbation is characterized by correlation function:

$$A^{-1}\int h(r-r_1)\,\mathrm{h(r)}\,dr = \Delta^2 e^{-\frac{r_1{}^2}{\Lambda^2}}$$

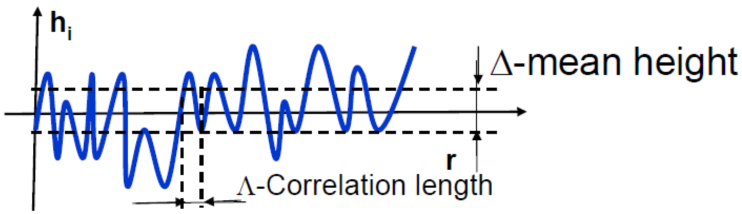

In Fourier Domain, the perturbation potential can be written as:

$$\left\langle \left|V_{q,n}\right|^2 \right\rangle = \Delta^2 \left(\sum_i \delta U^2\,(z_i) f_n(z_i) \right)^2 \Lambda^2 e^{-\frac{\Lambda^2 q^2}{4}}$$

Interface roughness scattering → τ_{IFR}

$$\hbar\tau_{21}{}^{-1} = \frac{\pi m^*}{\hbar^2}\Delta^2\Lambda^2\delta U^2 \sum_i \{f_2(z_i) f_1(z_i)\}^2 e^{\frac{-\Lambda^2 q_{21}{}^2}{4}}$$

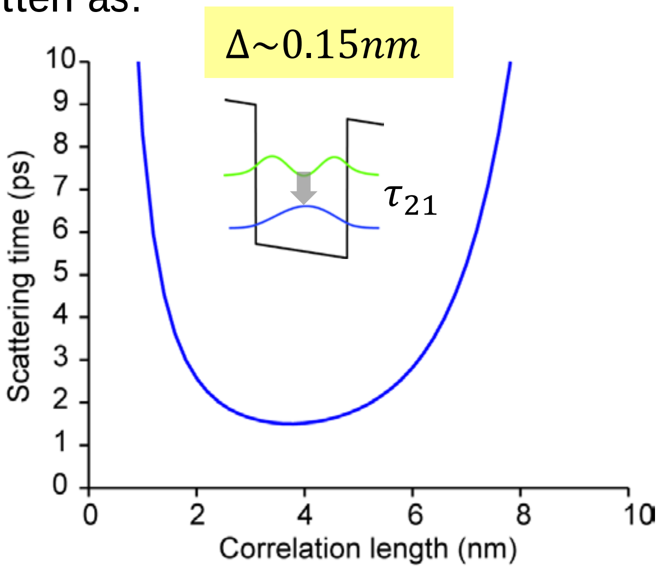

New Quantum Design: Ultra-strong Coupling

Before:

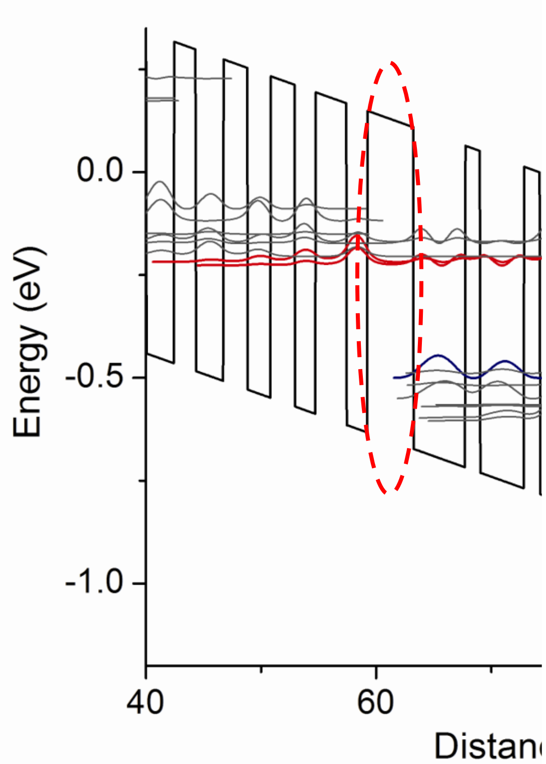

After:

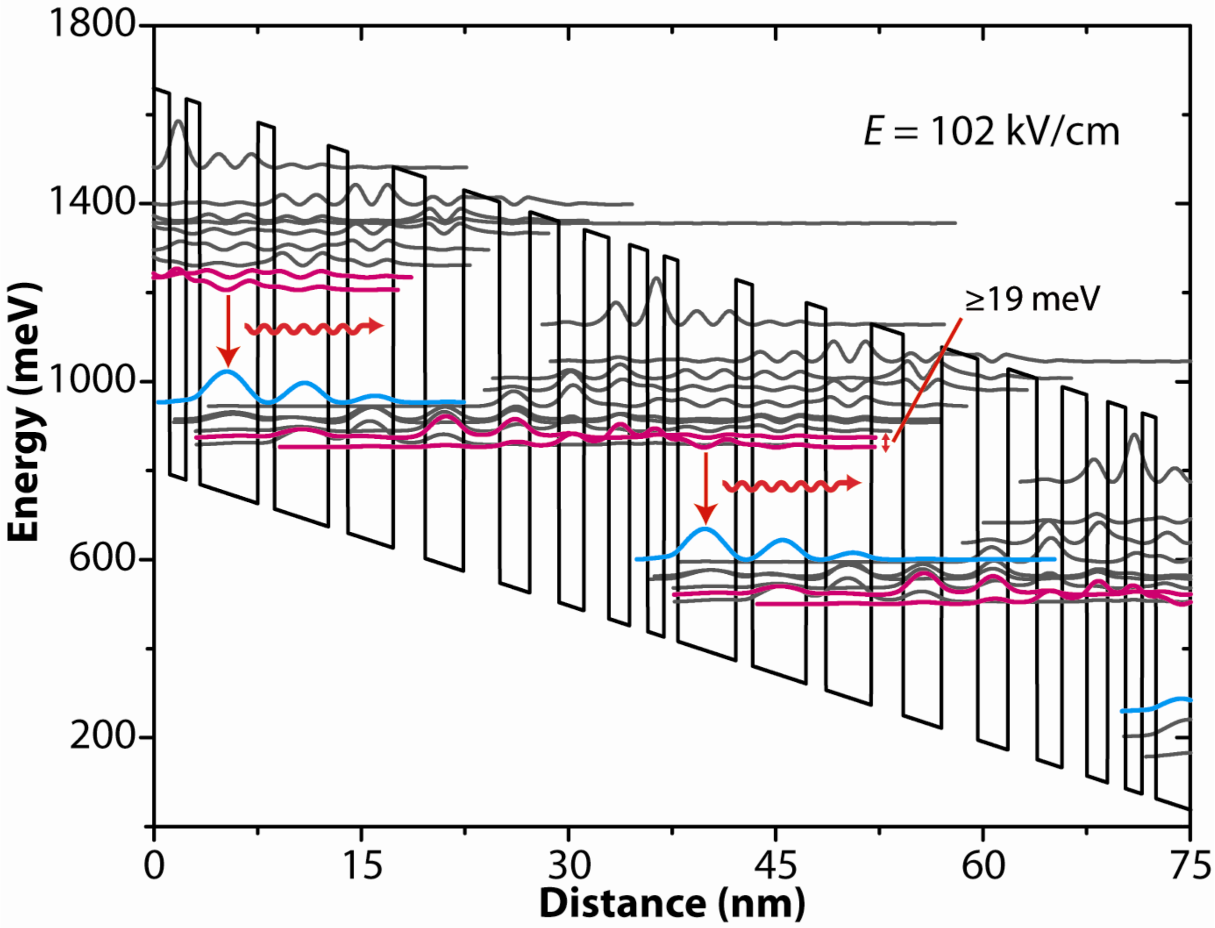

New QC Laser @ $\lambda \sim 4.7\ \mu m$

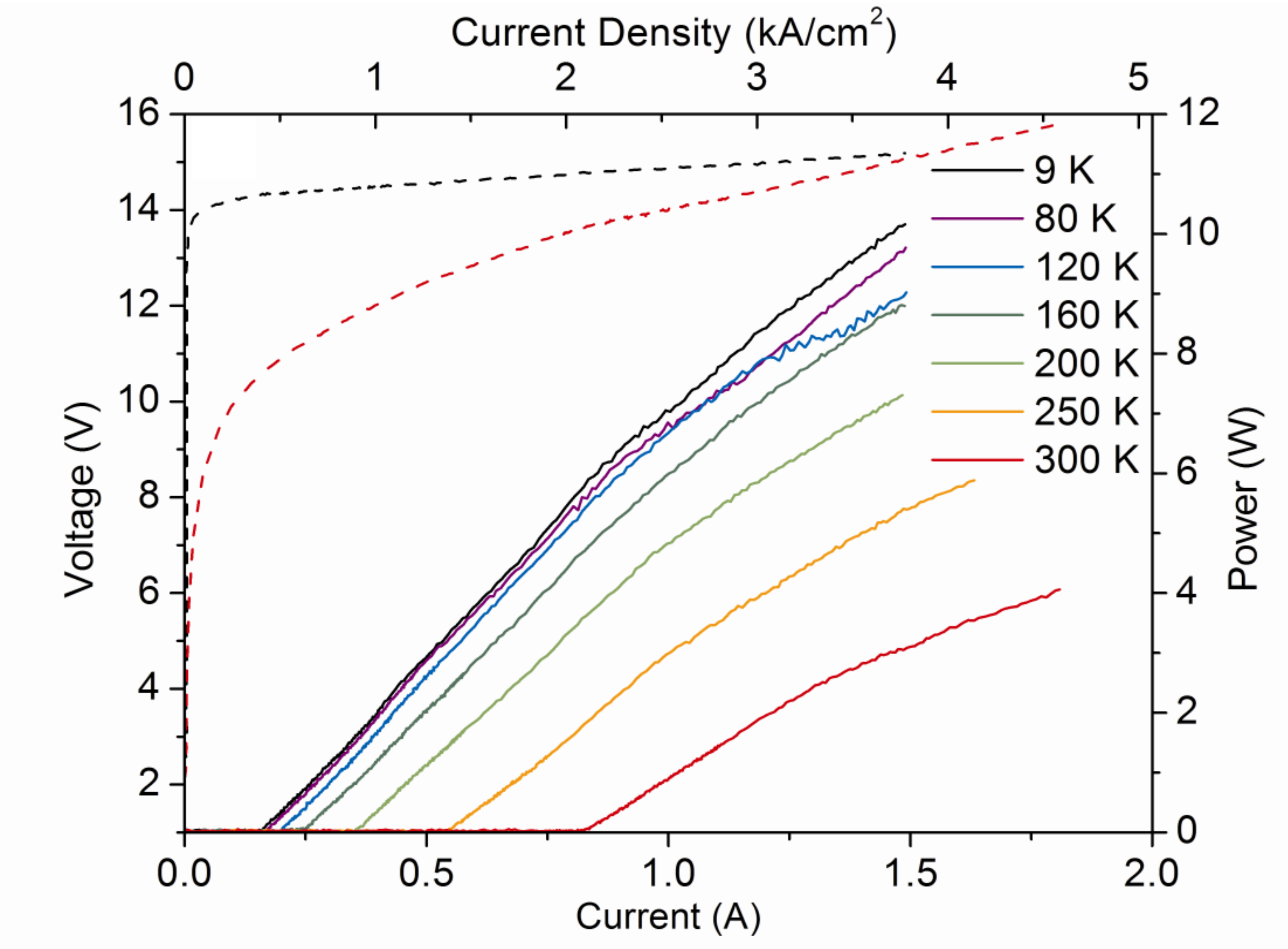

“Continuum-to-Continuum” Design

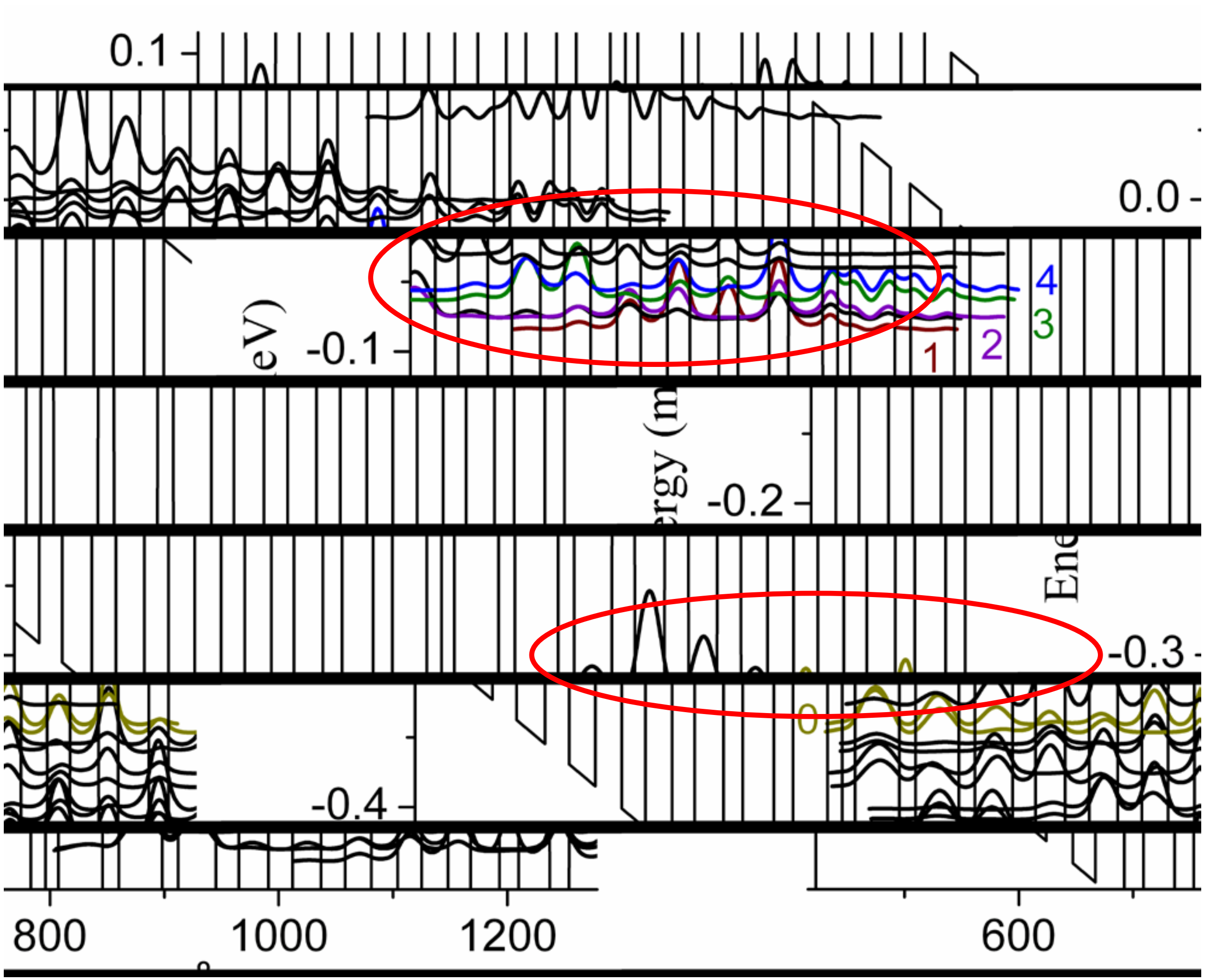

High Power Efficiency

$$WPE = \frac{\text{Light intensity}}{\text{Input power}}$$

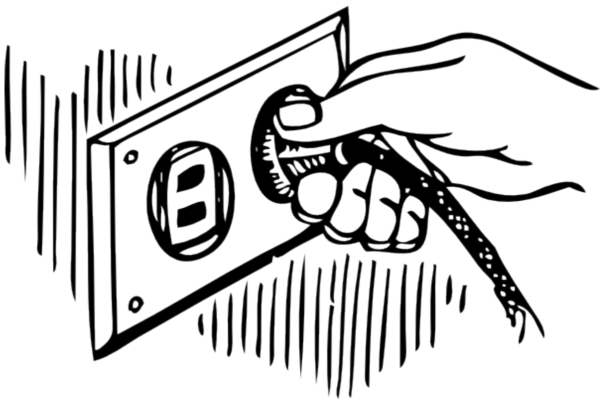

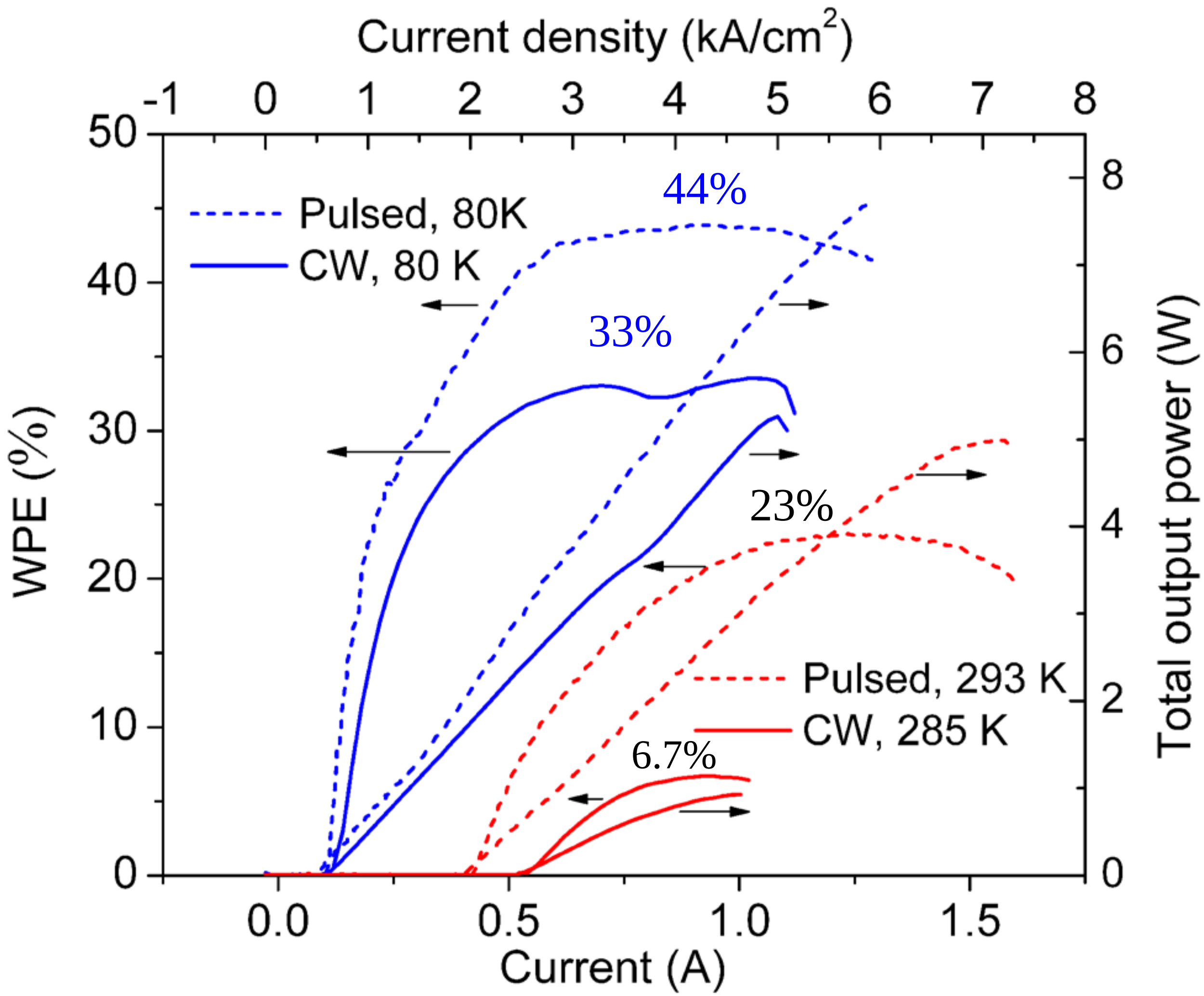

External Tuning: 4.4 - 5.2 µm

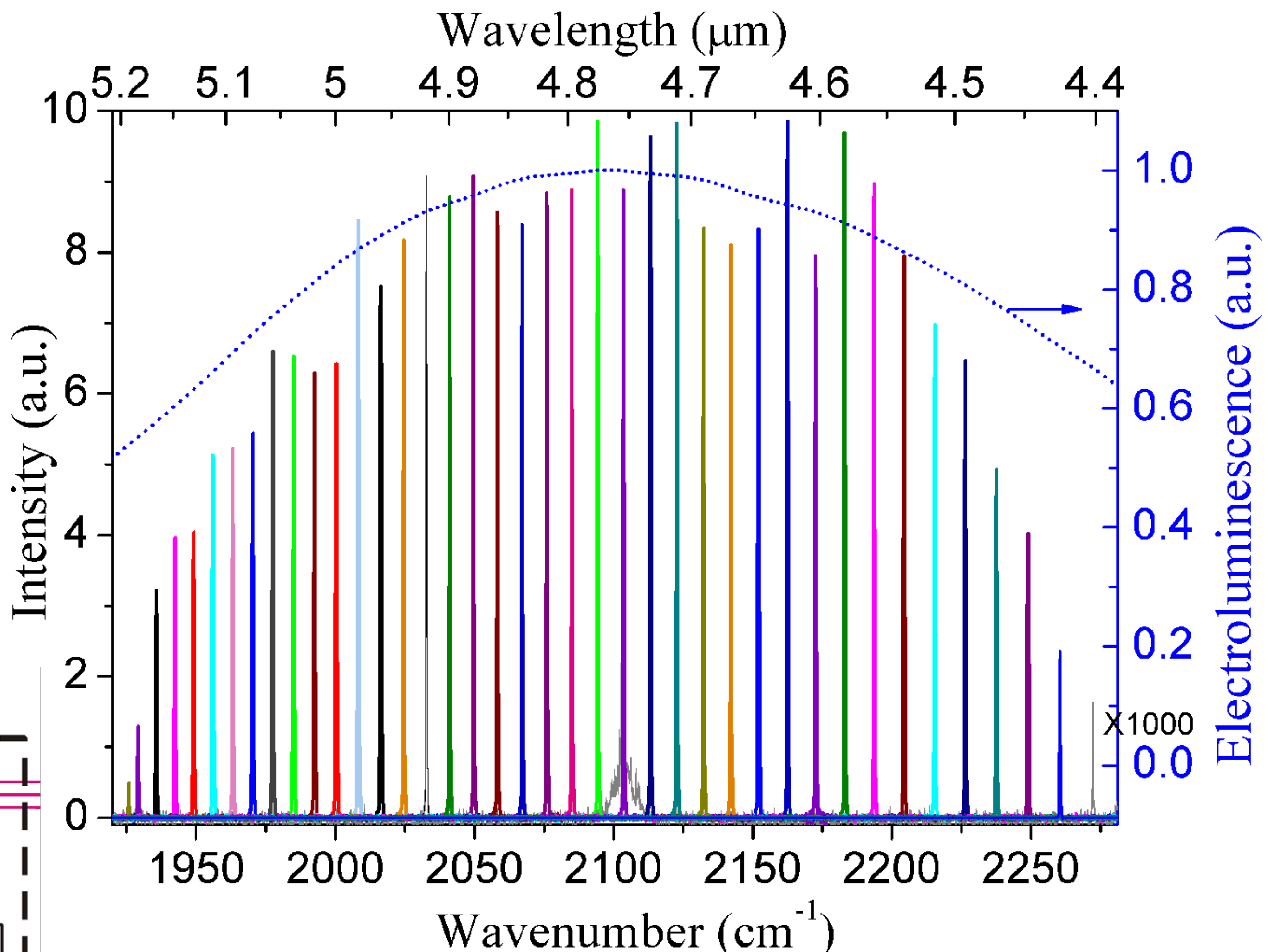

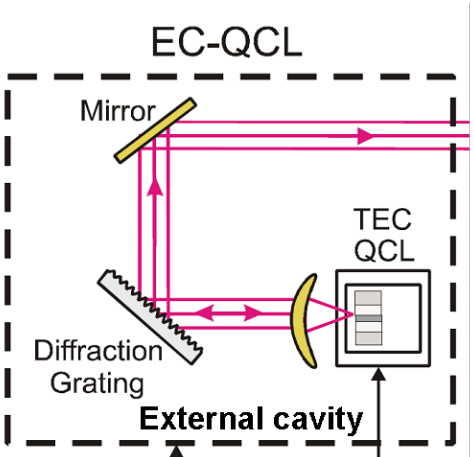

w/ Tracy Tsai, Gerard Wysocki et al.

Intersubband Lifetimes in QC lasers

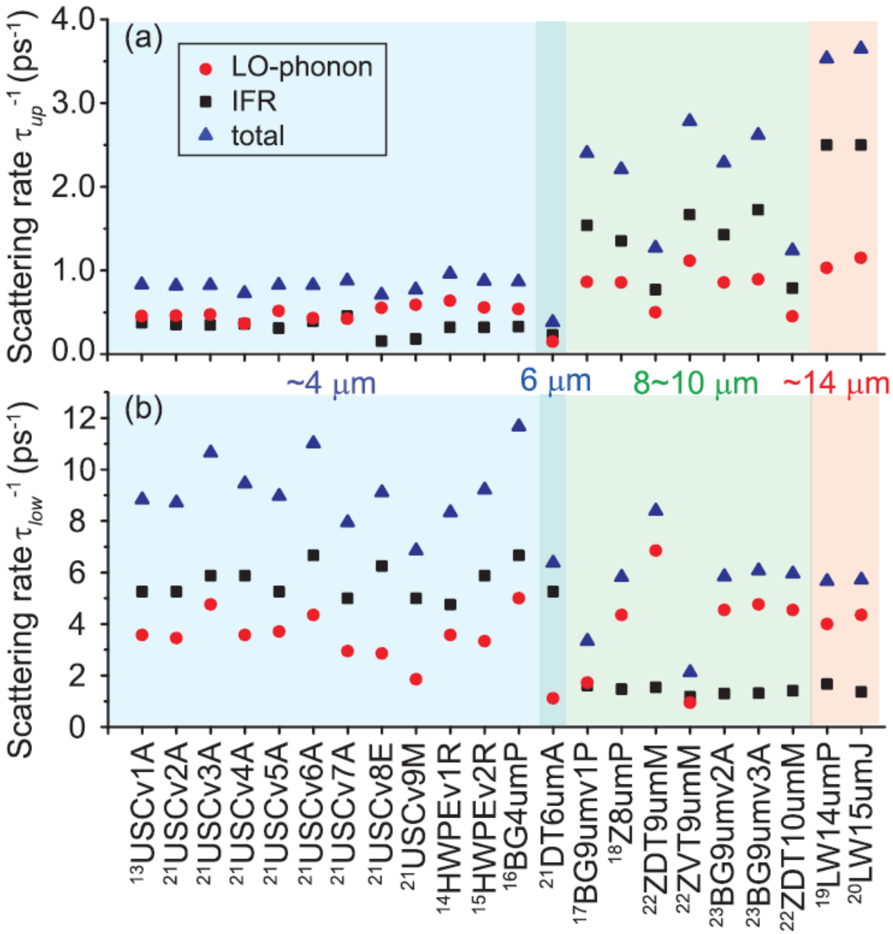

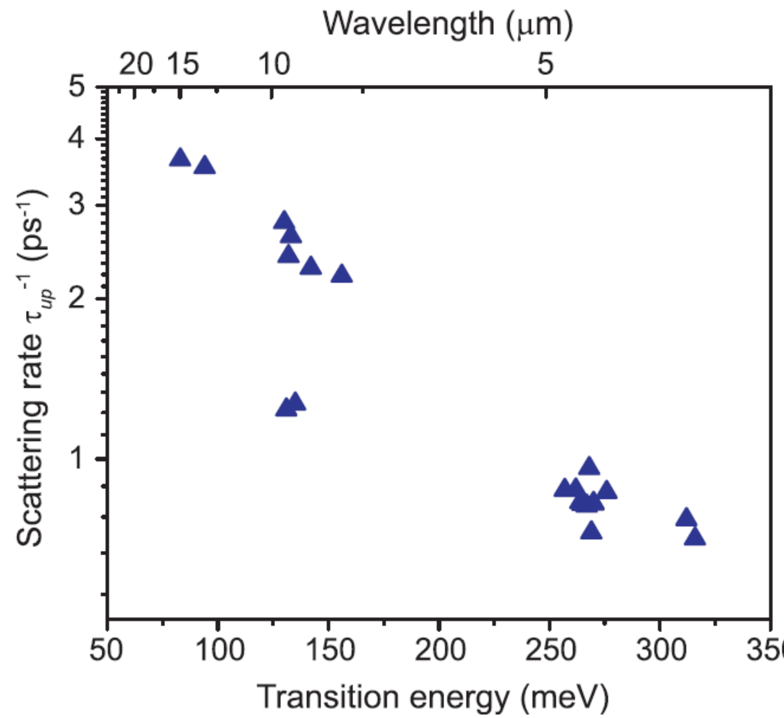

References in: YenTing Chiu et al. Appl. Phys. Lett. 101, 171117 (2012)

Upper Laser State Lifetime

- With a 2 level approximation and strong coupling between injector and upper laser state: $J_{max} = \frac{qN_s}{\tau_{transit}} \sim \frac{qN_s}{2\tau_3}$, while $2\tau_3 < \tau_{transit}$

- J_{max} can be determined from IV

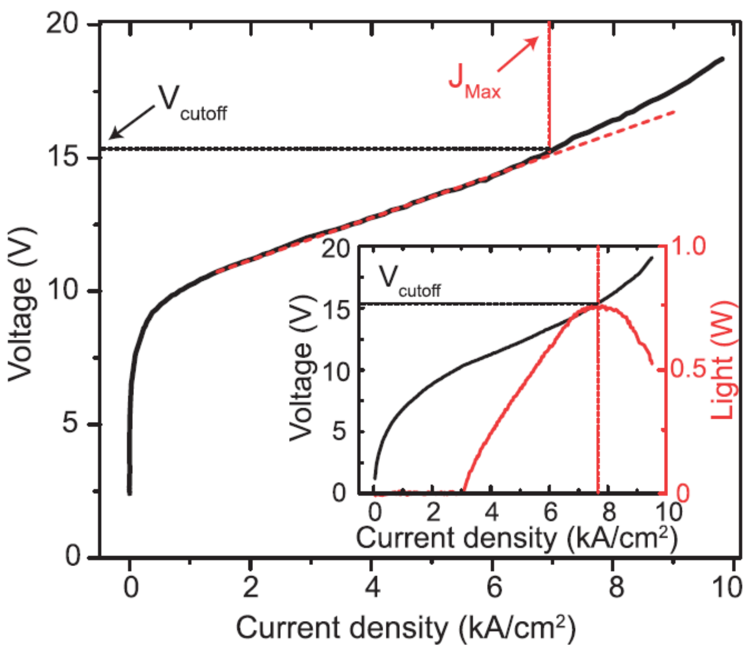

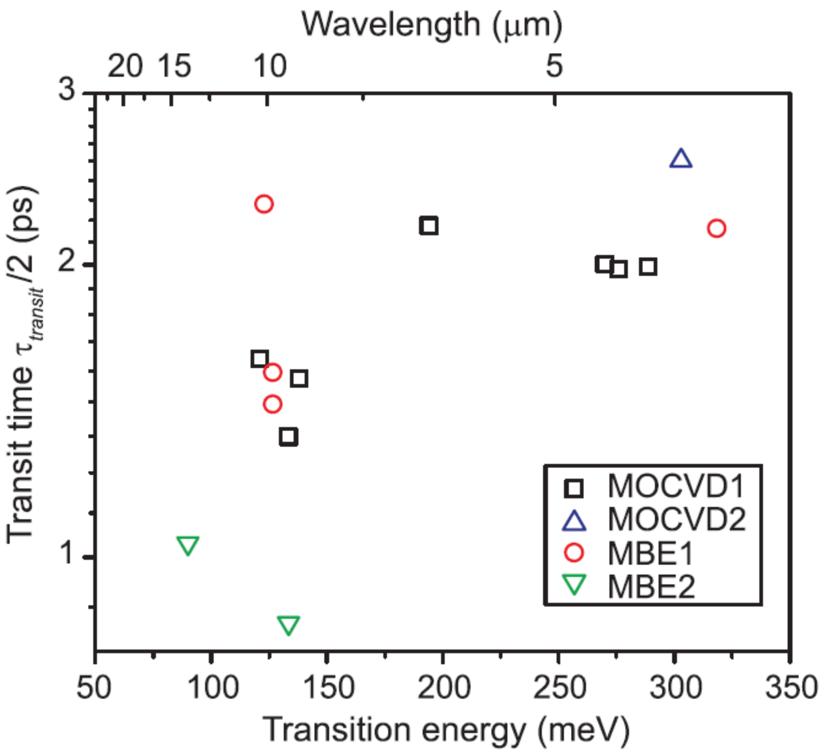

Comparison Model & Experiment

- Inclusion of interface roughness scattering provides better match:

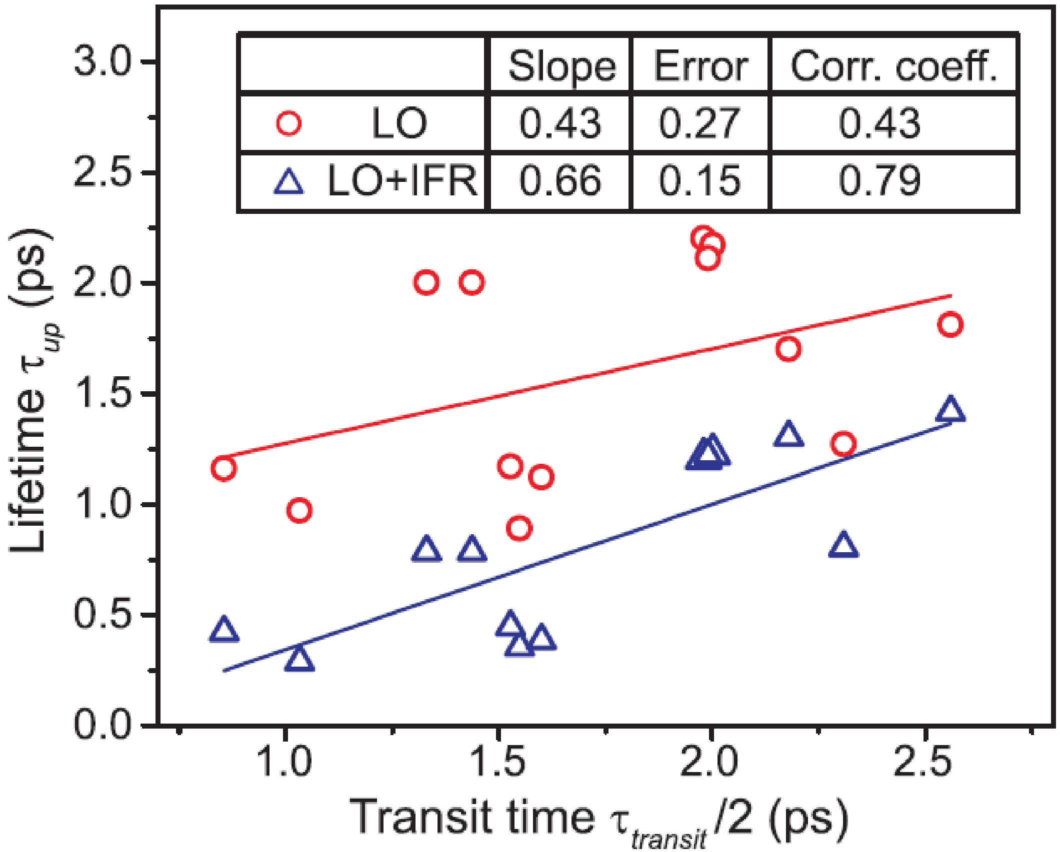

Same-wavelength cascaded-transition Quantum Cascade Laser

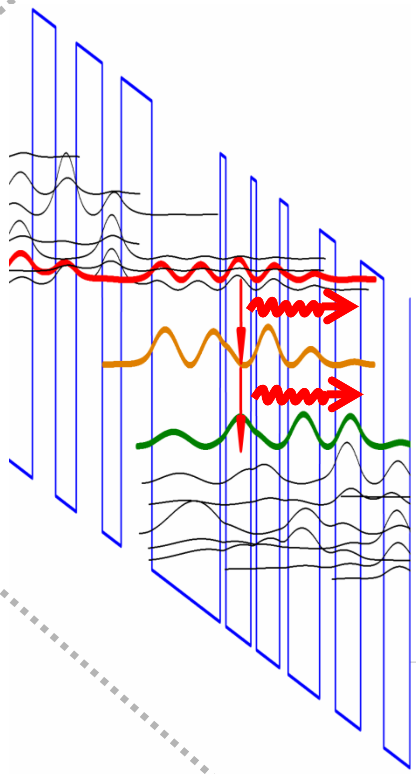

Xue Huang[1], *Jingyuan L. Zhang*[1], *William O. Charles*[1,2], *Vadim Tokranov*[3], *Serge Oktyabrsky*[3], *and Claire F. Gmachl*[1]

[1] Princeton University, Princeton, NJ 08544, US

[2] Current address: Phononic Devices, Inc., Raleigh, NC 27606, US

[3] University at Albany-SUNY, Albany, NY 12222, US

This work is supported in part by MIRTHE (NSF-ERC).

Cascaded-transition QC laser: review

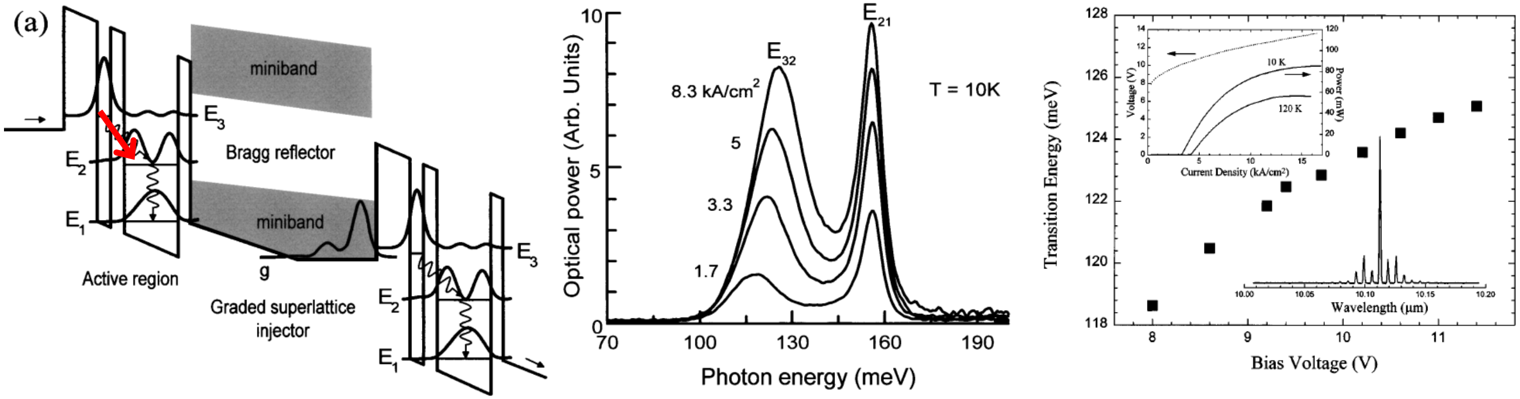

C. Sirtori et al., *Opt. Lett.* **23**, 463 (1998)

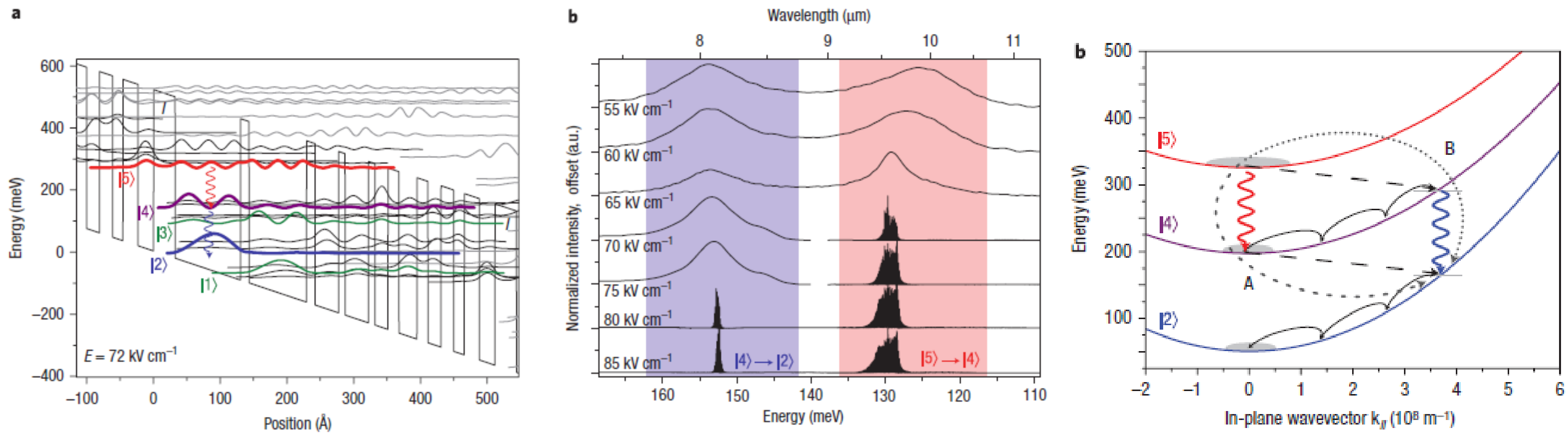

K. J. Franz et al., *Nature Photonics* **3**, 50-54 (2009)

Same-wavelength Cascaded-transition QC laser

- Same-wavelength cascaded transition

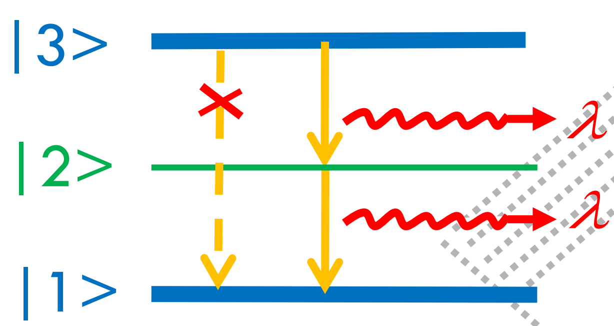

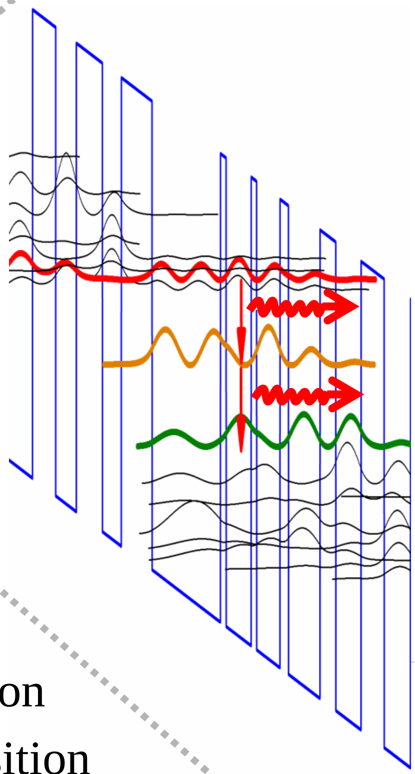

- Advantages:
  - Increased **quantum efficiency**
  - **Pumping and depopulation by stimulated emissions**

    First transition → **populate** the upper state of the second transition

    Second transition → **depopulate** the lower state of the first transition

Rate equations

$$\frac{dN_3}{dt}=\frac{J}{e}-\frac{N_3}{\tau_3}-\Gamma S_{32}\varphi\left(N_3-N_2\right)$$

$$\frac{dN_2}{dt}=\frac{N_3}{\tau_{32}}+\Gamma S_{32}\varphi\left(N_3-N_2\right)-\frac{N_2}{\tau_2}-\Gamma S_{21}\varphi\left(N_2-N_1\right)$$

$$\frac{dN_1}{dt}=\frac{N_2}{\tau_{21}}+\Gamma S_{21}\varphi\left(N_2-N_1\right)-\frac{N_1}{\tau_1}$$

$$\frac{d\varphi}{dt}=\frac{c}{n}\varphi[\frac{\Gamma S_{32}\left(N_3-N_2\right)+\Gamma S_{21}\left(N_2-N_1\right)}{L_p}-\alpha]$$

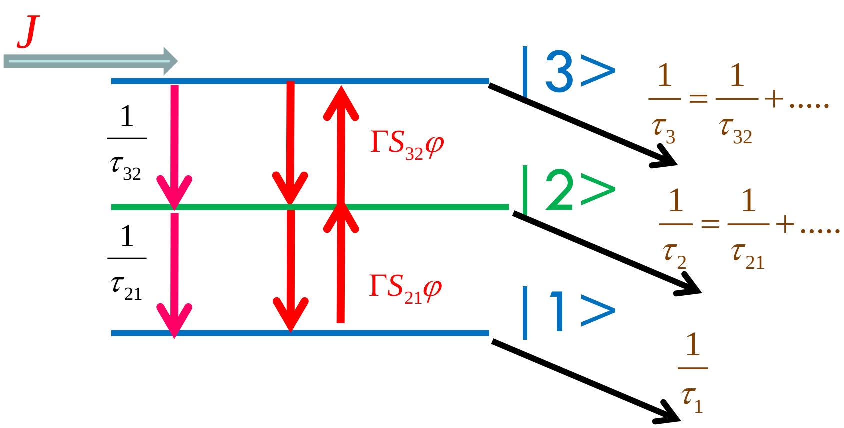

$N_1,\ N_2,\ N_3$: electron sheet density per period

$\tau_1,\ \tau_2,\ \tau_3$: lifetime

$\tau_{32},\ \tau_{21}$: scattering lifetime

Γ : confinement factor

L_p : thickness of a period

α : total loss

cross section:

$$S_{32}=\frac{4\pi e z_{32}^2}{\lambda_0\varepsilon_0 n L_p}\frac{1}{2\hbar\gamma_{32}},\quad S_{21}=\frac{4\pi e z_{21}^2}{\lambda_0\varepsilon_0 n L_p}\frac{1}{2\hbar\gamma_{21}}$$

z_{32}, z_{21} : dipole matrix elements; $z_{31}\approx 0$

$2\hbar\gamma_{21},\ 2\hbar\gamma_{32}$: linewidth

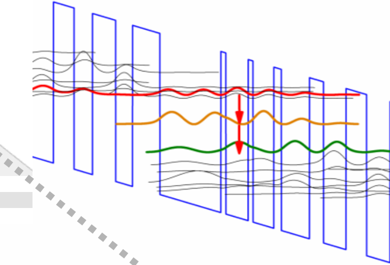

Active region design

Cascaded-transition active core

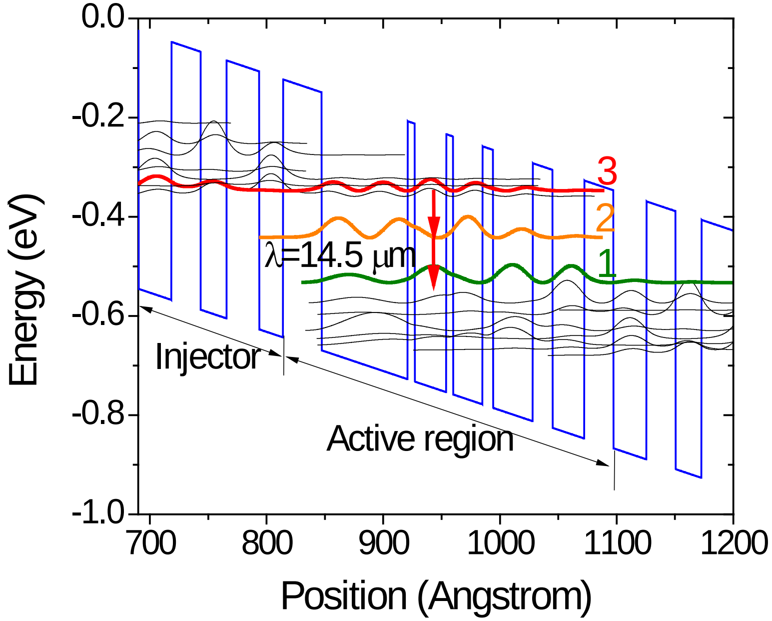

$z_{32} = 3.3\,nm$; $z_{21} = 4.0\,nm$;

$\tau_{32} = 2.5\,ps$; $\tau_{21} = 1.8\,ps$;

$\tau_3 = 1.4\,ps$; $\tau_2 = 0.6\,ps$; $\tau_1 = 0.2\,ps$.

Single- transition active core

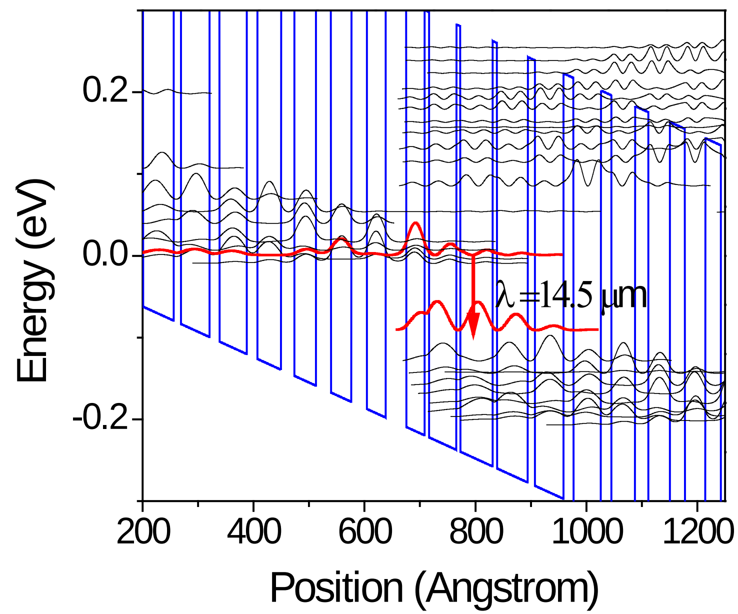

$z_{32} = 2.6\,nm$; $\tau_{32} = 3.1\,ps$;

$\tau_3 = 1.6\,ps$; $\tau_2 = 0.2\,ps$.

Calculated gain coefficient: $\frac{g_{cascaded}}{g_{single}} = 2.4$

Simulated lasing characteristics

Light output comparison

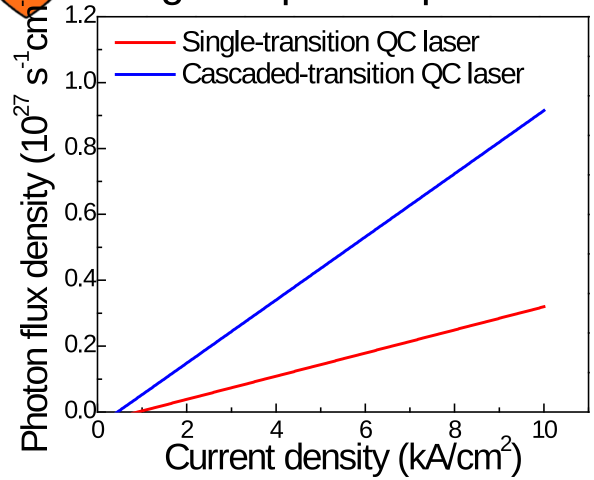

Population Inversion

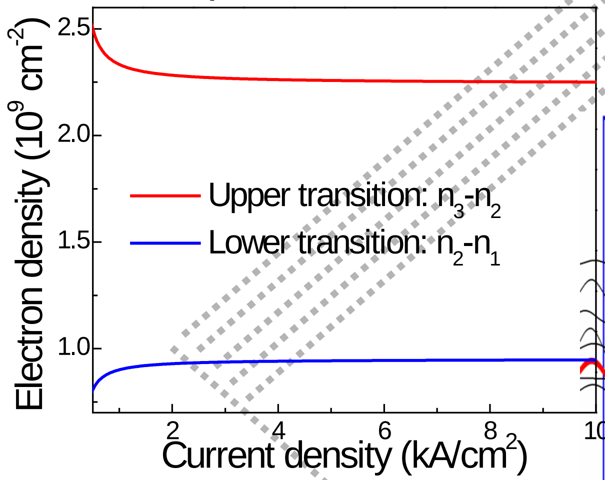

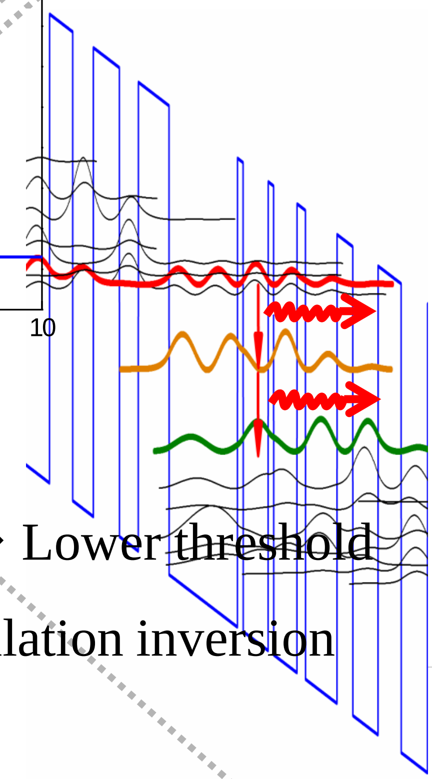

Laser gain

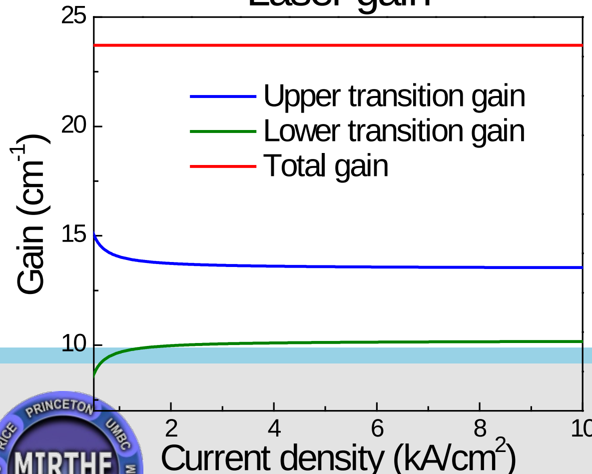

- Higher gain coefficient → Lower threshold
- Nonlinear change in population inversion and gain

Characterization

Light- Current- Voltage

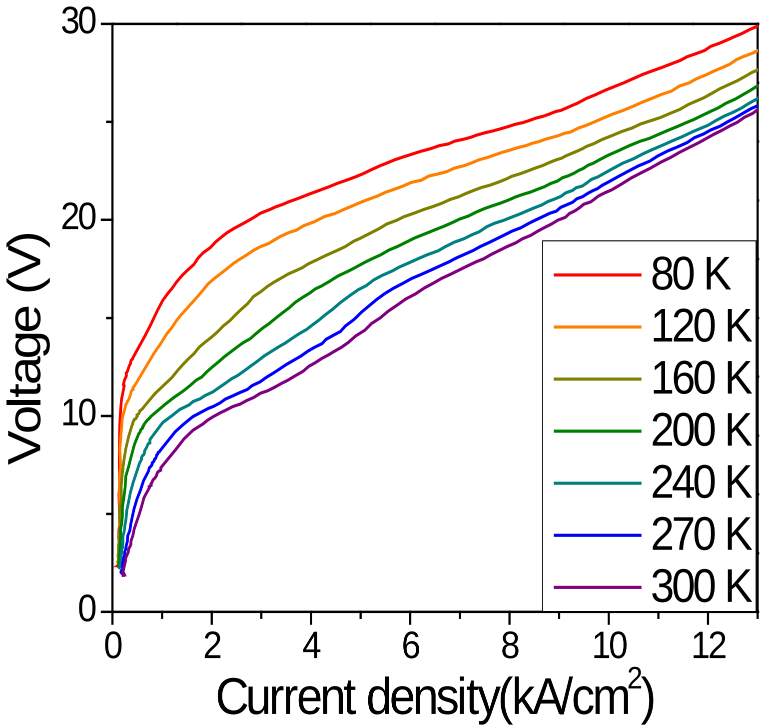

Electroluminescence at 80 K

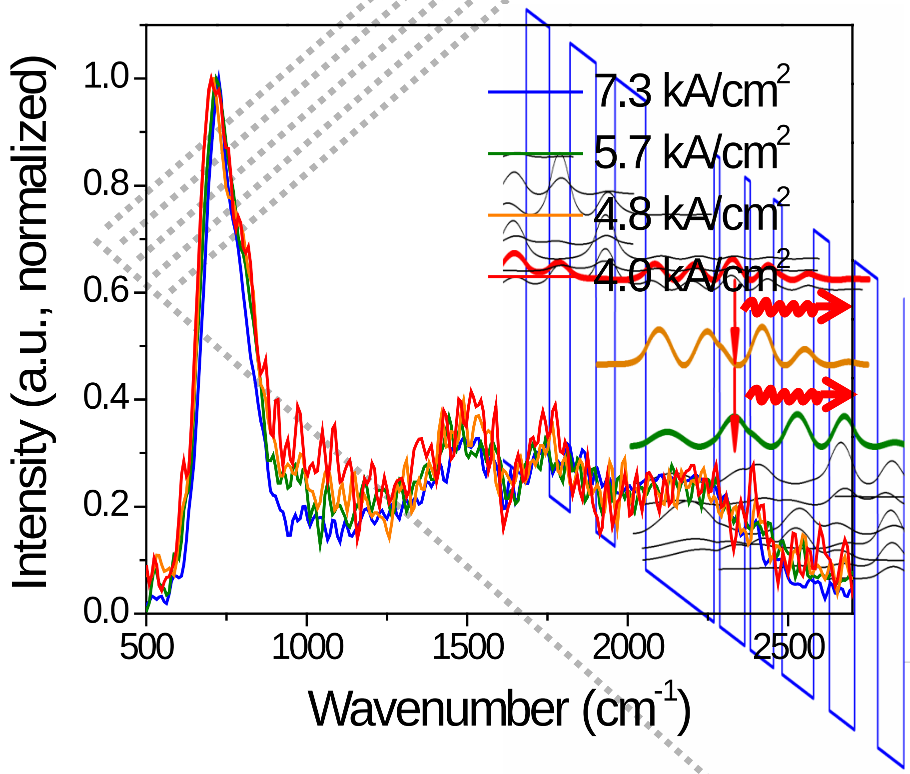

Stacked structure: waveguide design

➢Cascaded-transition amplifier

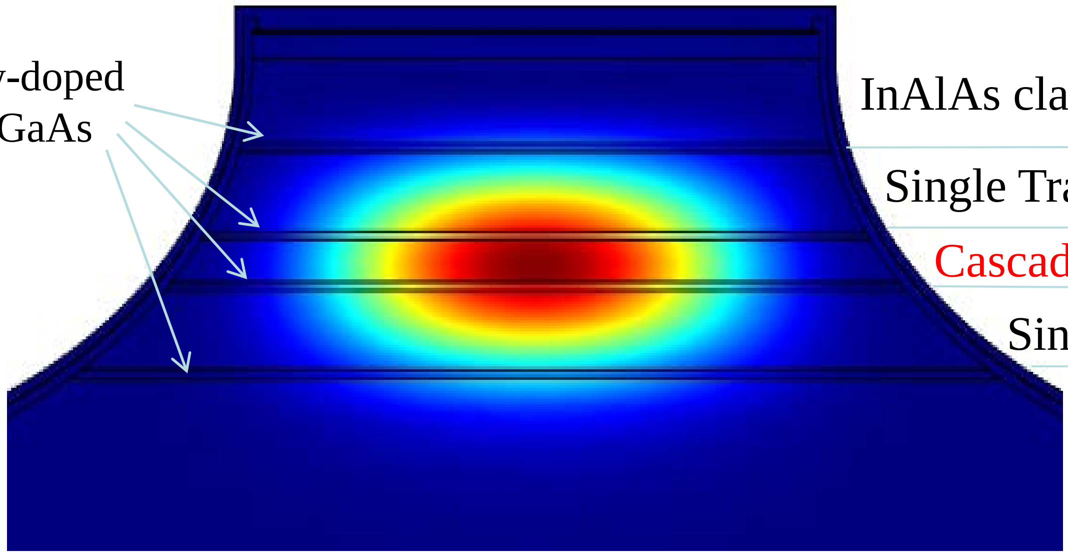

➢**Confinement factor**:

Cascaded transition: 23.3%

Single transition: 55.9%

Electroluminescence and laser spectra

Electroluminescence at 80 K

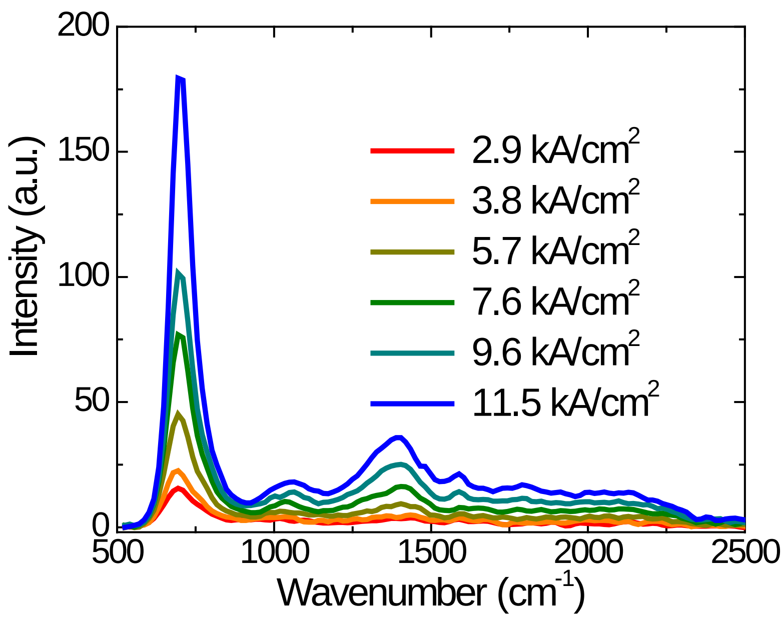

Main peak: 690 cm^{-1} (14.5 μm)

Main spurious peak: 1388 cm^{-1} (7.2 μm)

Ridge laser spectra

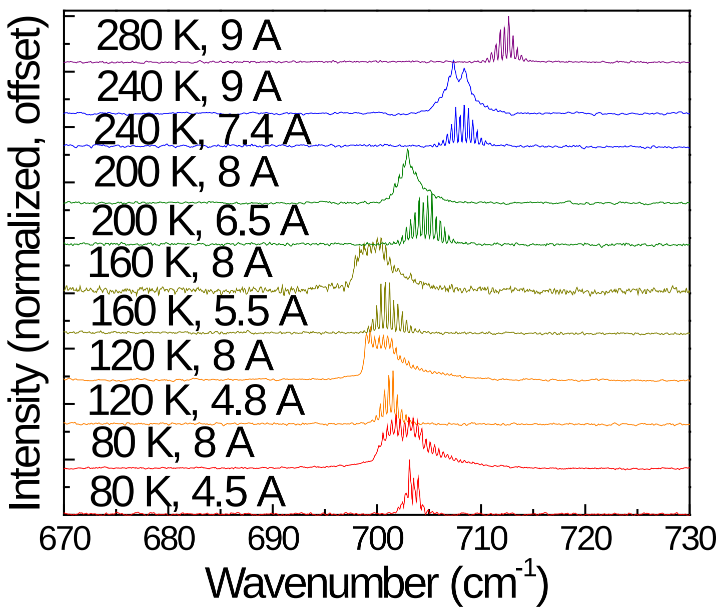

3.4 mm long, 23 μm wide laser

Light – Current – Voltage characteristics

Light-Current-Voltage (LIV)

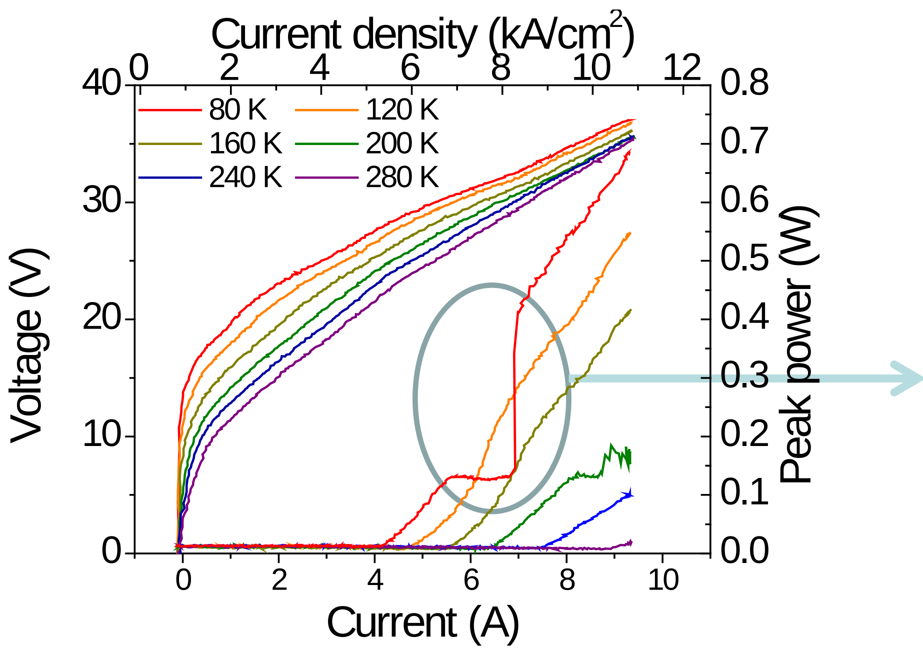

Step change in power output

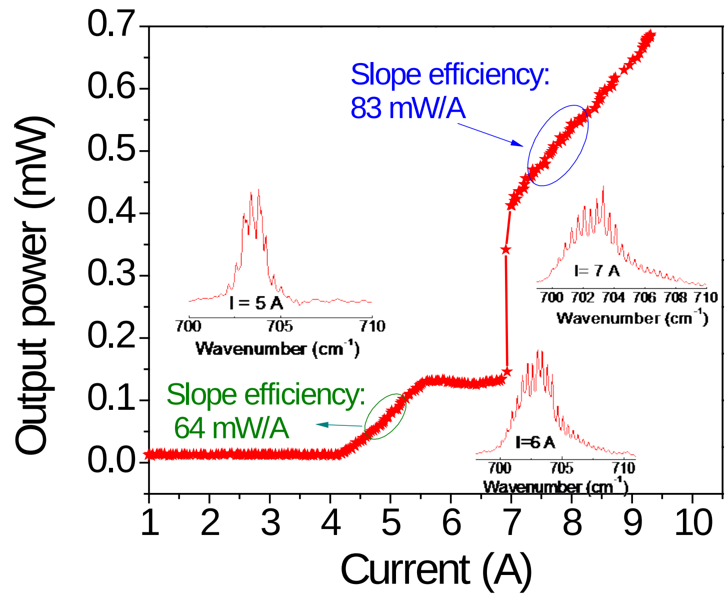

- ➢ **Slope efficiency increased by 30%**
- ➢ **No change in center wavelength**

Rate equations

Cascaded Transition

$$\frac{dN_{c,3}}{dt}=\eta_u\frac{J}{e}-\frac{N_{c,3}}{\tau_{c,3}}-\Gamma_c S_{c,32}\varphi\left(N_{c,3}-N_{c,2}\right)$$

$$\frac{dN_{c,2}}{dt}=\eta_m\frac{J}{e}+\frac{N_{c,3}}{\tau_{c,32}}+\Gamma_c S_{32}\varphi\left(N_{c,3}-N_{c,2}\right)-\frac{N_{c,2}}{\tau_{c,2}}-\Gamma_c S_{c,21}\varphi\left(N_{c,2}-N_{c,1}\right)$$

$$\frac{dN_{c,1}}{dt}=\frac{N_{c,2}}{\tau_{c,21}}+\Gamma_c S_{c,21}\varphi\left(N_{c,2}-N_{c,1}\right)-\frac{N_{c,1}}{\tau_{c,1}}$$

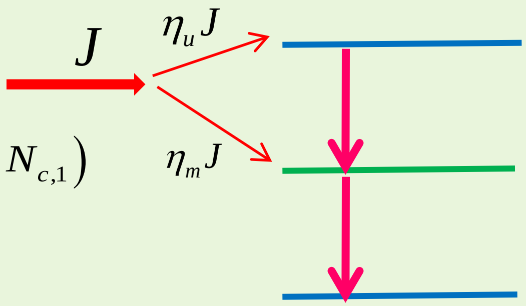

Single Transition

$$\frac{dN_{s,3}}{dt}=\frac{J}{e}-\frac{N_{s,3}}{\tau_{s,3}}-\Gamma_s S_{s,32}\varphi\left(N_{s,3}-N_{s,2}\right)$$

$$\frac{dN_{s,1}}{dt}=\frac{N_{s,2}}{\tau_{s,21}}+\Gamma_s S_{s,21}\varphi\left(N_{s,2}-N_{s,1}\right)-\frac{N_{s,1}}{\tau_{s,1}}$$

$$\frac{d\varphi}{dt}=\frac{c}{n}\varphi\left[\frac{\Gamma_c S_{c,32}\left(N_{c,3}-N_{c,2}\right)+\Gamma_c S_{c,21}\left(N_{c,2}-N_{c,1}\right)}{L_c}+\frac{\Gamma_s S_{s,32}\left(N_{s,3}-N_{s,2}\right)}{L_s}-\alpha\right]$$

"Phase transition"

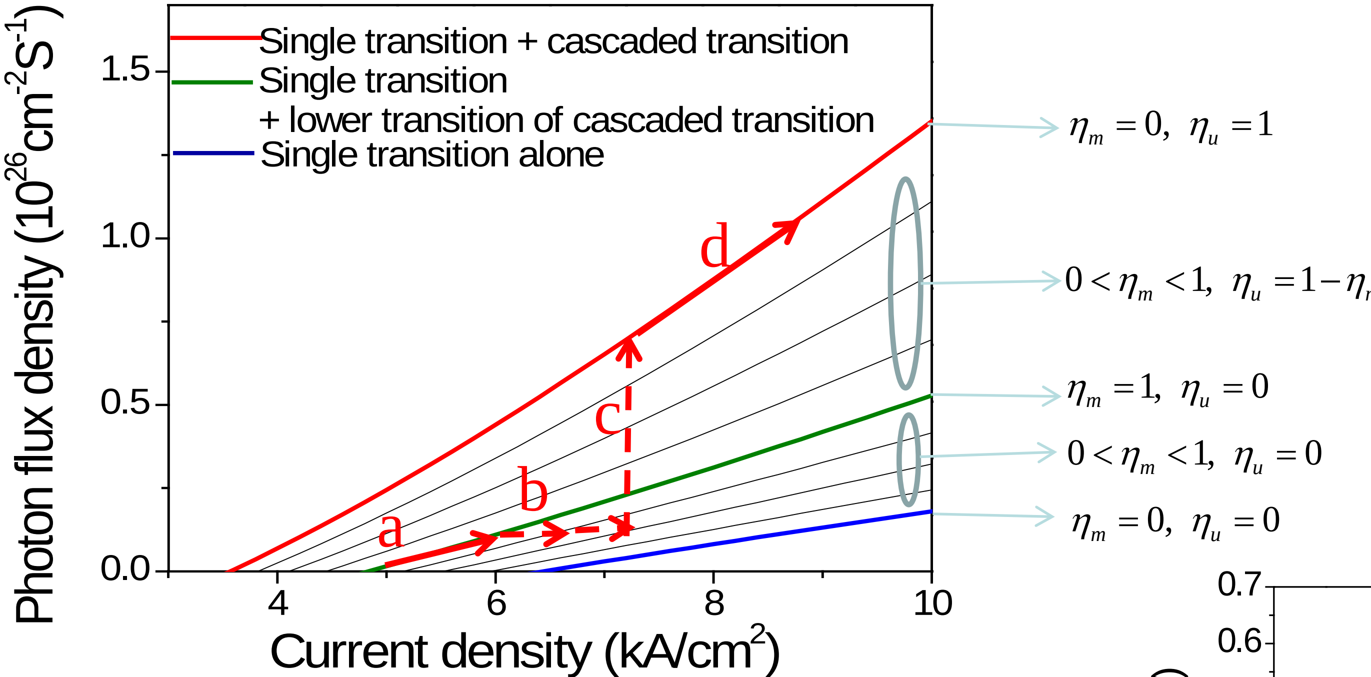

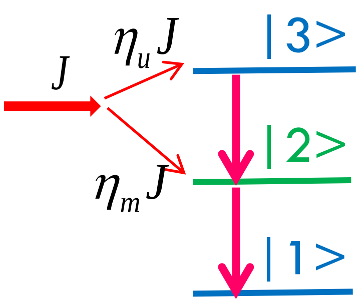

Current injection for cascaded-transition stack

- Phase a: in resonance with the middle state |2>
- Phase b: off resonance, partial injection into |2>
- Phase c: transition to resonance with the upper state |3>
- Phase d: in resonance with |3>

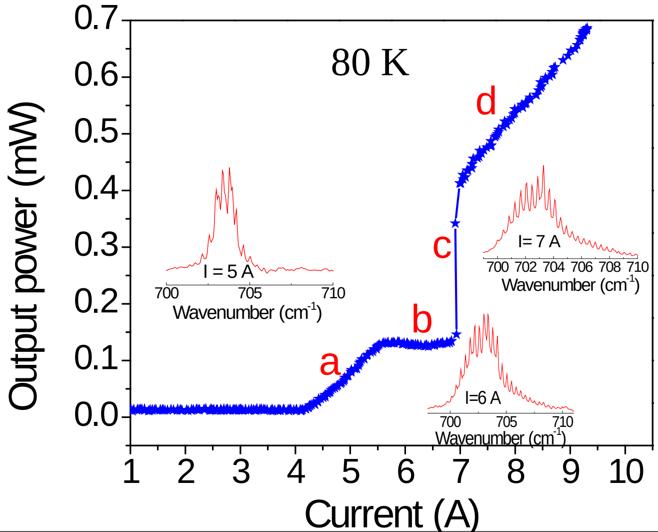

New directions in cavity design

Single-mode Quantum Cascade Lasers Employing an Asymmetric Mach-Zehnder Interferometer Type Cavity

Peter Q. Liu[1], Xiaojun Wang[2], Jen-Yu Fan[2], Claire F. Gmachl[1]

[1]Department of Electrical Engineering, Princeton University, Princeton, NJ 08544 USA
[2]AdTech Optics, 18007 Cortney Court, City of Industry, CA 91748 USA

Funding support: MIRTHE NSF-ERC, DARPA EMIL, Princeton University

FP Cavity QCL vs. Single-mode QCL

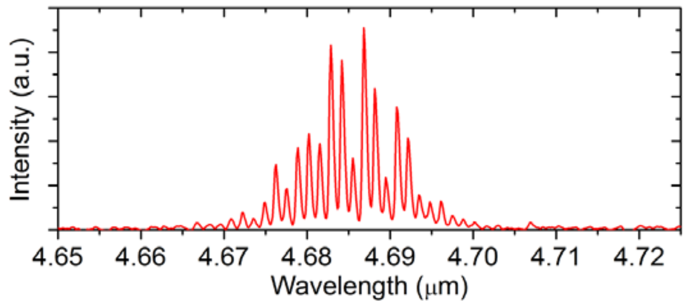

Conventional Fabry-Perot cavity QCLs

- Relative simple fabrication → relatively low cost
- High throughput, high yield
- Generally not single-mode

Single-mode QCLs

DFB QCLs

- Complicated and time-consuming fabrication
- Relatively lower throughput

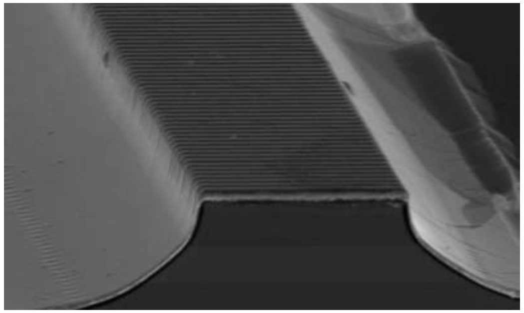

Courtesy of Loan Le

External cavity QCLs

- Require high-precision optical alignment
- Higher cost and less compact

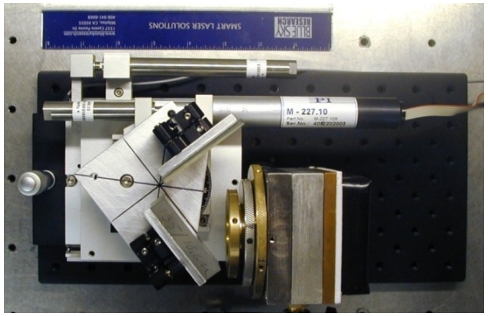

Courtesy of Tracy Tsai

Monolithic coupled-cavity QCLs

- Fabrication identical to simple ridge lasers
- High throughput, low cost, robust
- Significant coupling loss → high lasing threshold

P.Q. Liu et al., *APL* **98**, 061110 (2011)

P.Q. Liu et al., *APL* **99**, 241112 (2011)

Wavelength Selectivity of Asymmetric Mach-Zehnder Interferometer

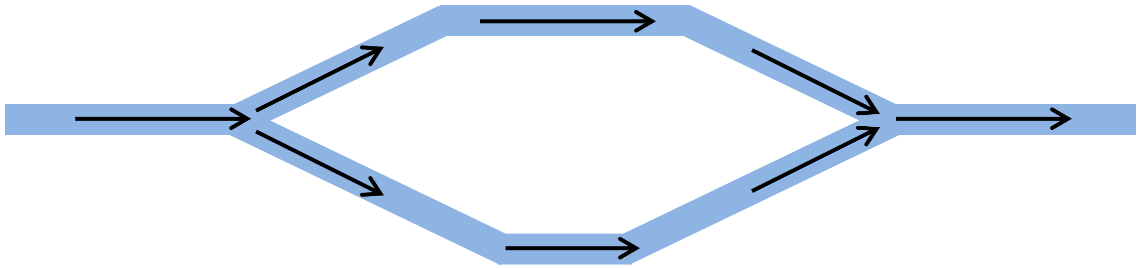

- The two arms of the AMZ interferometer have a length difference ΔL.
- Light entering the AMZ interferometer is split equally into the two arms, and recombined at the other end with a phase difference $\Delta\Phi = 2\pi n_{eff} k_m \Delta L$.
- If $\Delta\Phi = 2\mathrm{N}\pi$, light from the two arms interfere constructively →peak transmission.

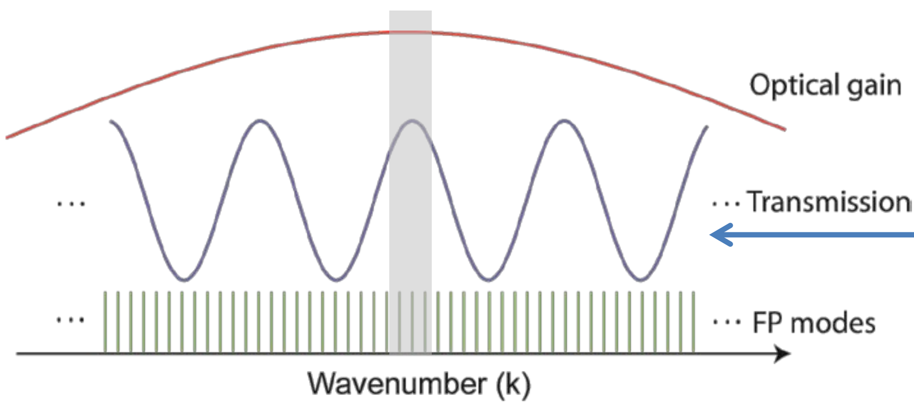

AMZ interferometer transmission:

$$\mathrm{T}(k) = \cos^2(n_{eff} k \Delta L \pi)$$

Period of transmission peaks:

$$dk = \frac{1}{n_{eff}\Delta L}$$

- The lasing modes are selected by three factors: the optical gain spectrum, the FP cavity and the AMZ interferometer.

Initial Cavity Design and Device Fabrication

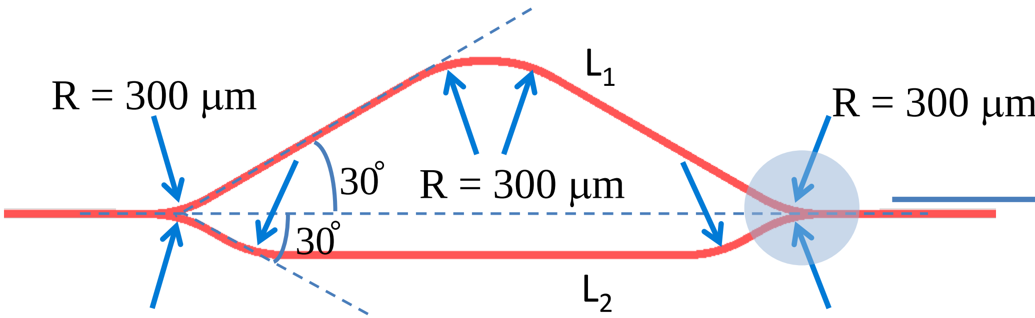

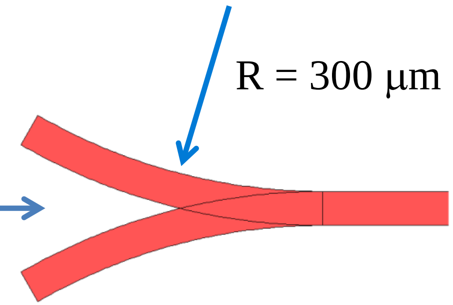

Four different initial designs:

ΔL = 50 μm, 65 μm, 100 μm, 150 μm

$L_{avg} = (L_1+L_2)/2 \approx$ 1.2 mm, 1.3 mm, 1.5mm, 1.8 mm

Ridge width: ~10 μm

FSR of FP modes: $\frac{1}{2n_{eff}(L_R + L_{avg})}$

- ✓ Adiabatic transitions minimize coupling loss
- ✓ Monolithic structures
- ✓ Fully compatible with ridge laser fabrication

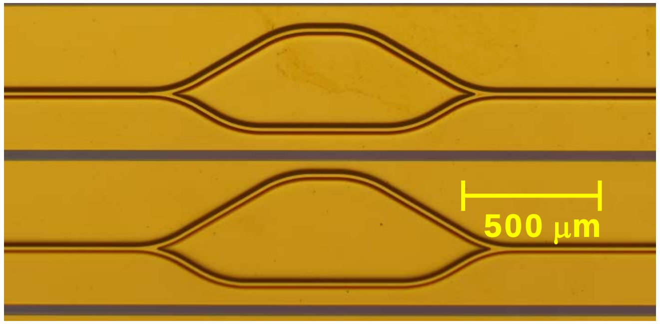

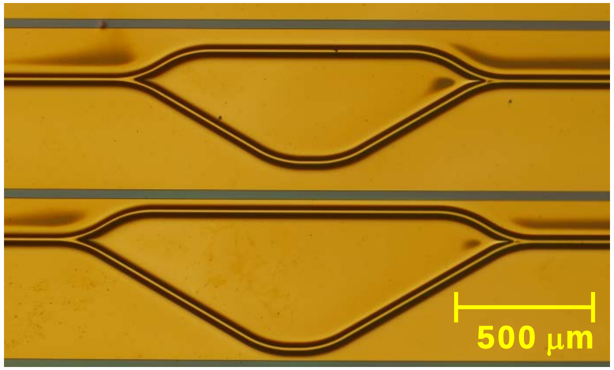

MIRTHE

Optimization of Cavity Designs

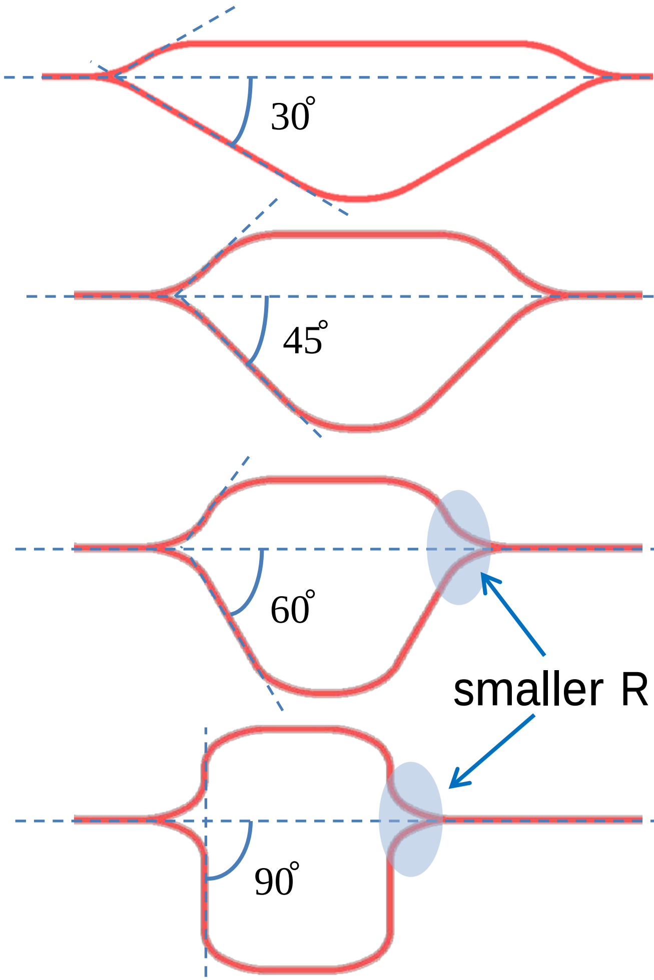

ΔL = 150 μm
$(L_1+L_2)/2 \approx 1.8$ mm

ΔL = 200 μm
$(L_1+L_2)/2 \approx 1.6$ mm

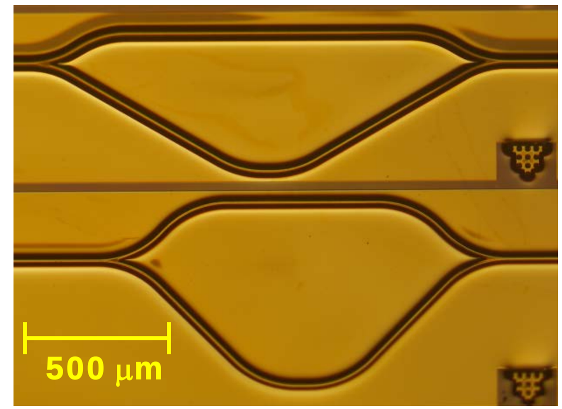

ΔL = 300 μm
$(L_1+L_2)/2 \approx 1.5$ mm

ΔL = 400 μm
$(L_1+L_2)/2 \approx 1.5$ mm

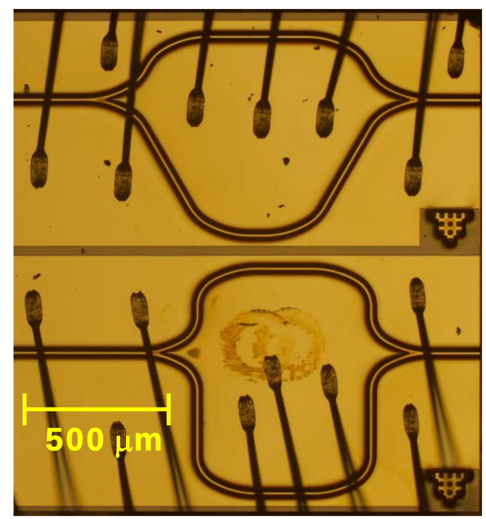

Device Characterization: Single-mode Operation

ΔL = 400 μm, total length ~1.4 mm

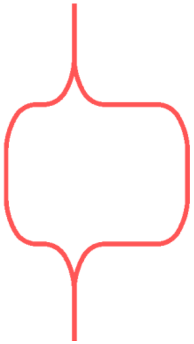

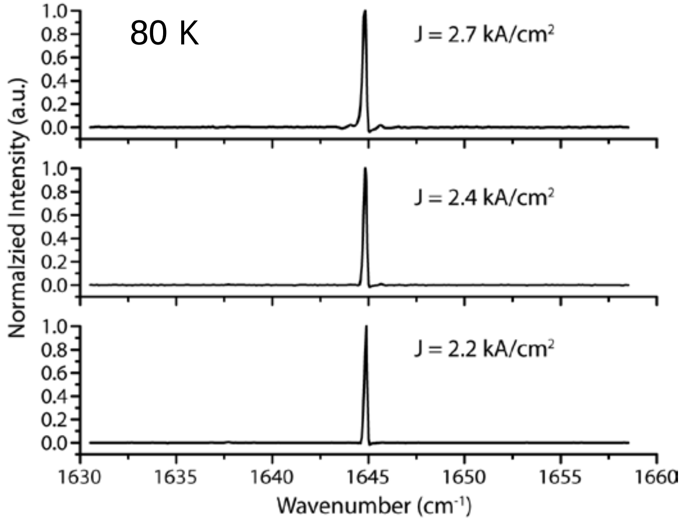

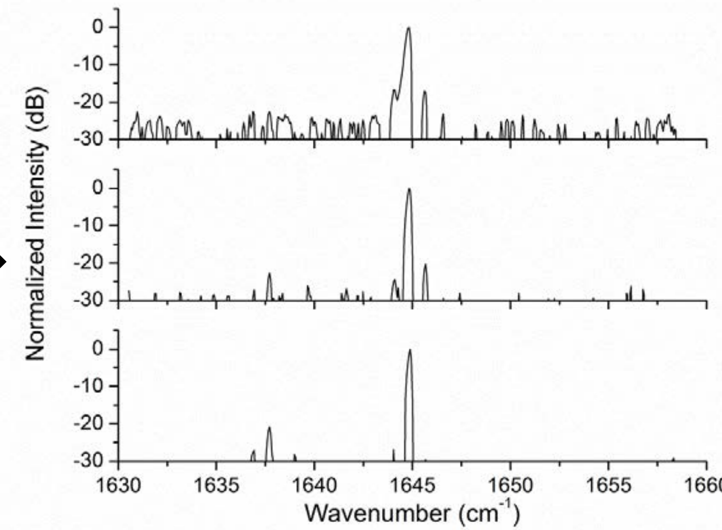

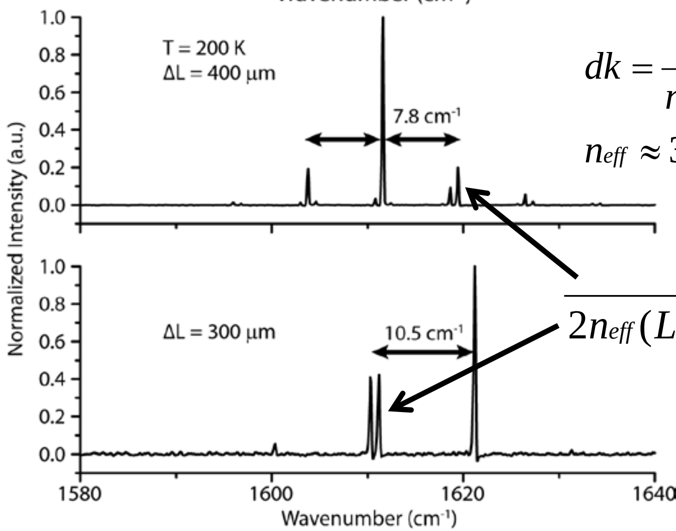

$$dk = \frac{1}{n_{eff}\Delta L}$$

$$n_{eff} \approx 3.2$$

$$\frac{1}{2n_{eff}(L_R + L_{avg})}$$

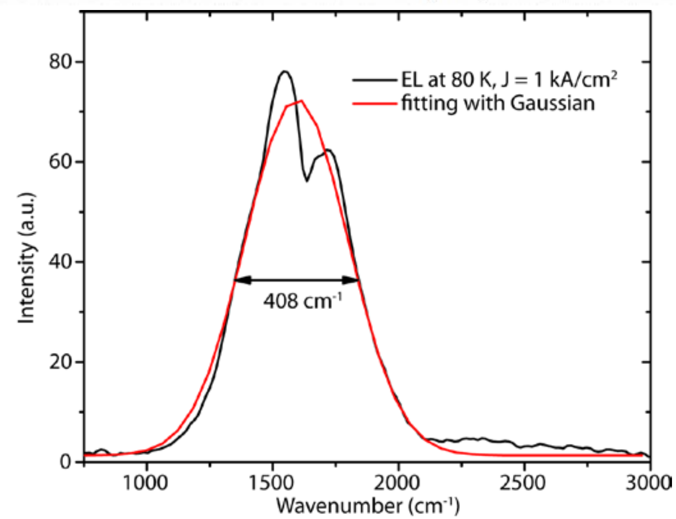

Single-mode Wavelength Tuning: CW Current Tuning

ΔL = 450 μm, device total length ~2.4 mm, back-facet HR coating

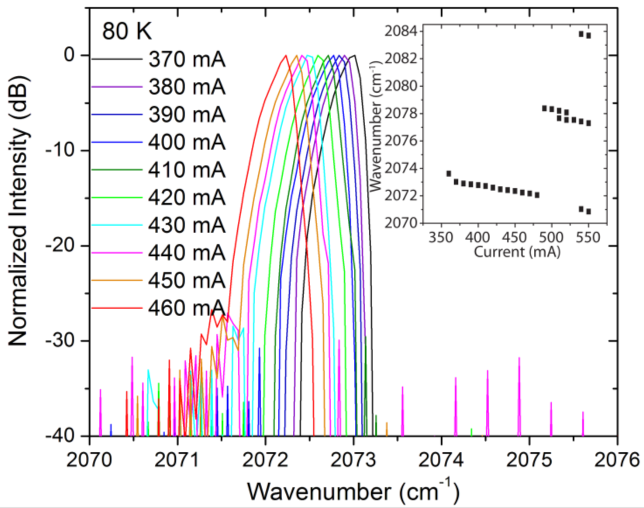

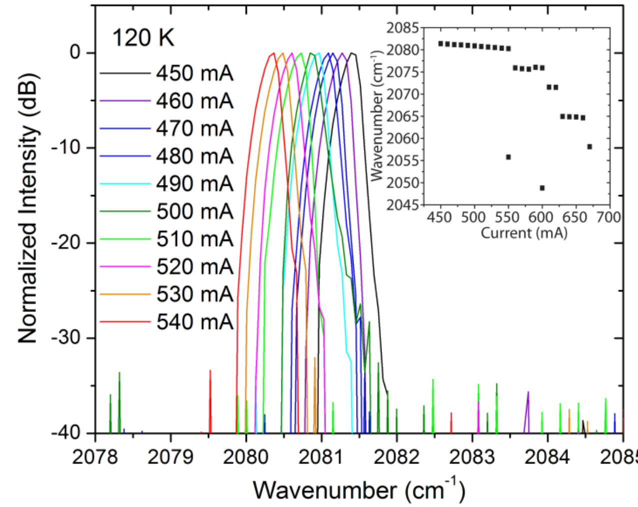

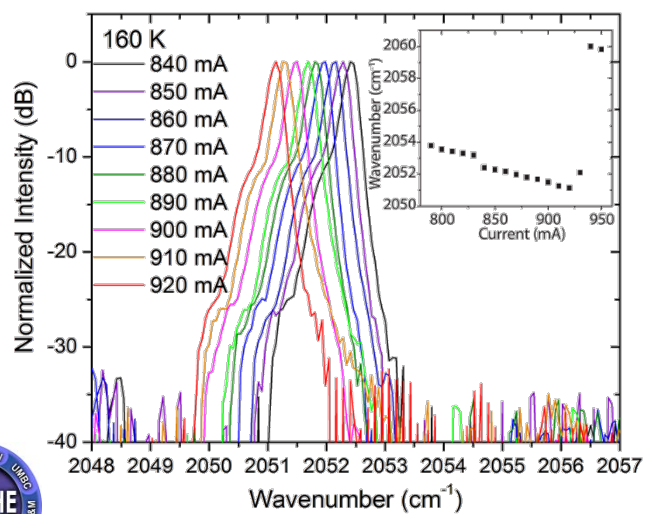

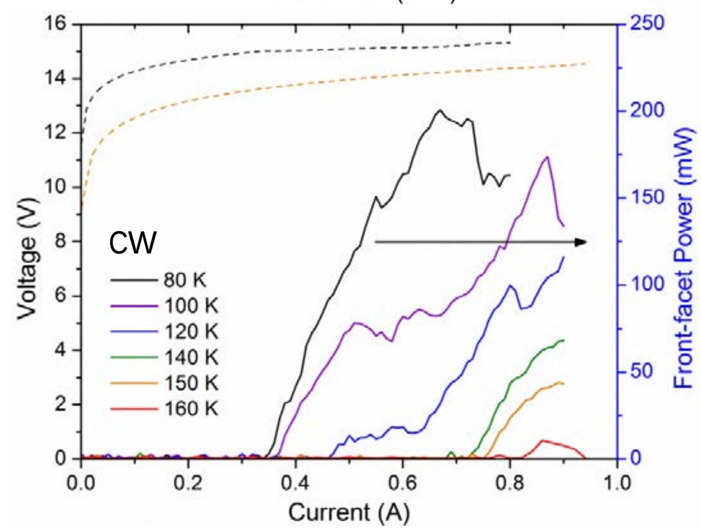

New directions in systems implementations

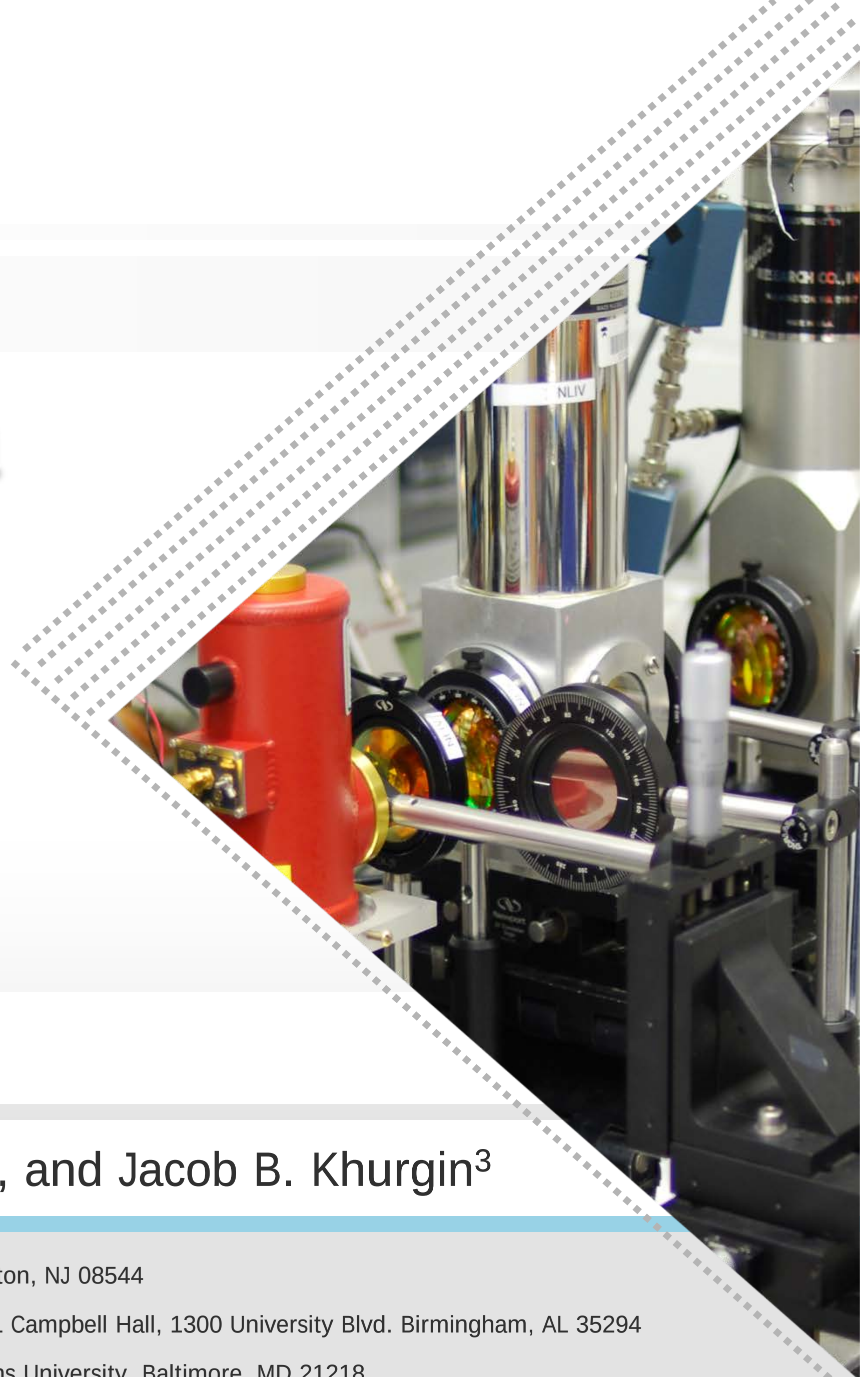

Yu Song[1]*, Sergey B. Mirov[2], Claire F. Gmachl[1], and Jacob B. Khurgin[3]

[1]Department of Electrical Engineering, Princeton University, Princeton, NJ 08544

[2]Department of Physics, University of Alabama at Birmingham, 421 Campbell Hall, 1300 University Blvd. Birmingham, AL 35294

[3]Department of Electrical and Computer Engineering, Johns Hopkins University, Baltimore, MD 21218

Introduction & Sample

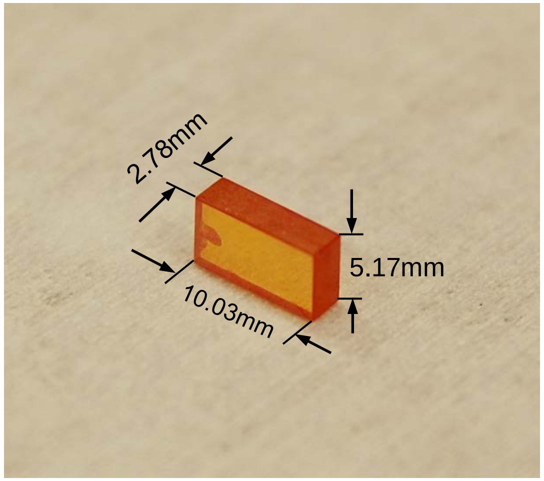

- Fe^{2+} doped ZnSe polycrystal
  - ❑ Chemical vapor transport growth technique
  - ❑ Post-growth thermal diffusion doping
    - Fe^{2+} (1.5×10^{19} cm^{-3}).
  - ❑ The sample was cut and polished

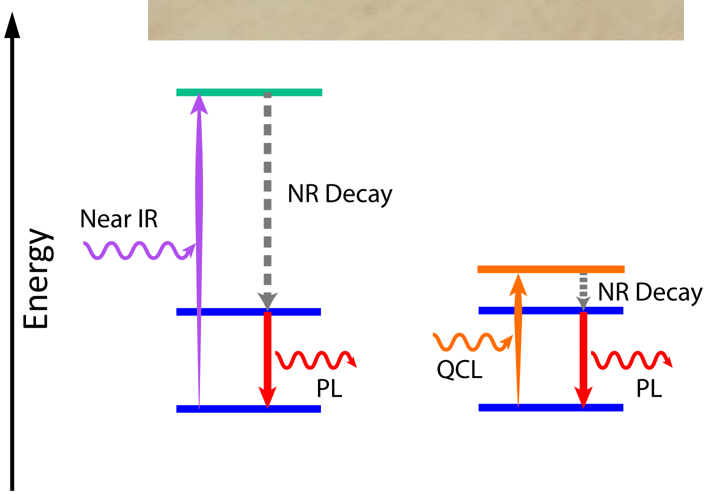

- *Growth: Prof Sergey B. Mirov*

Field Campaign in Ghana 2009 /2010

Fishing village of Elmina

Wood pile used in fish smoking

Chorkor Smoker- oven used in fish smoking

2010 QCLOPS Sensor Setup

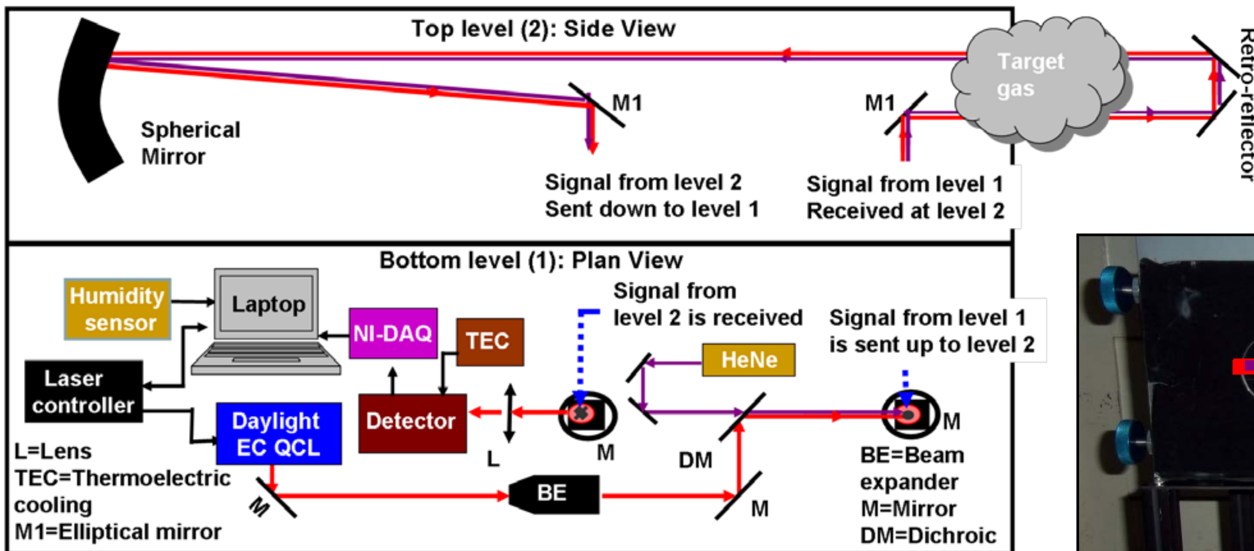

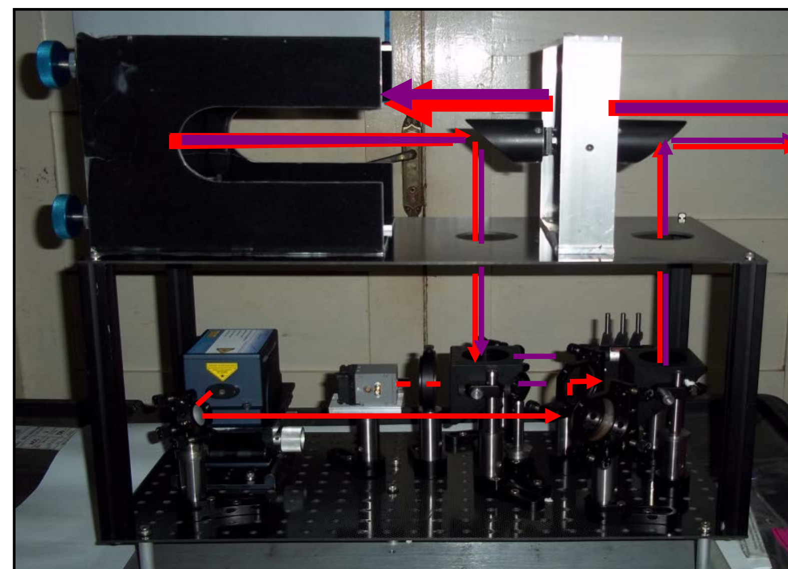

2 x 1 ft

2010 Field Campaign - Elmina

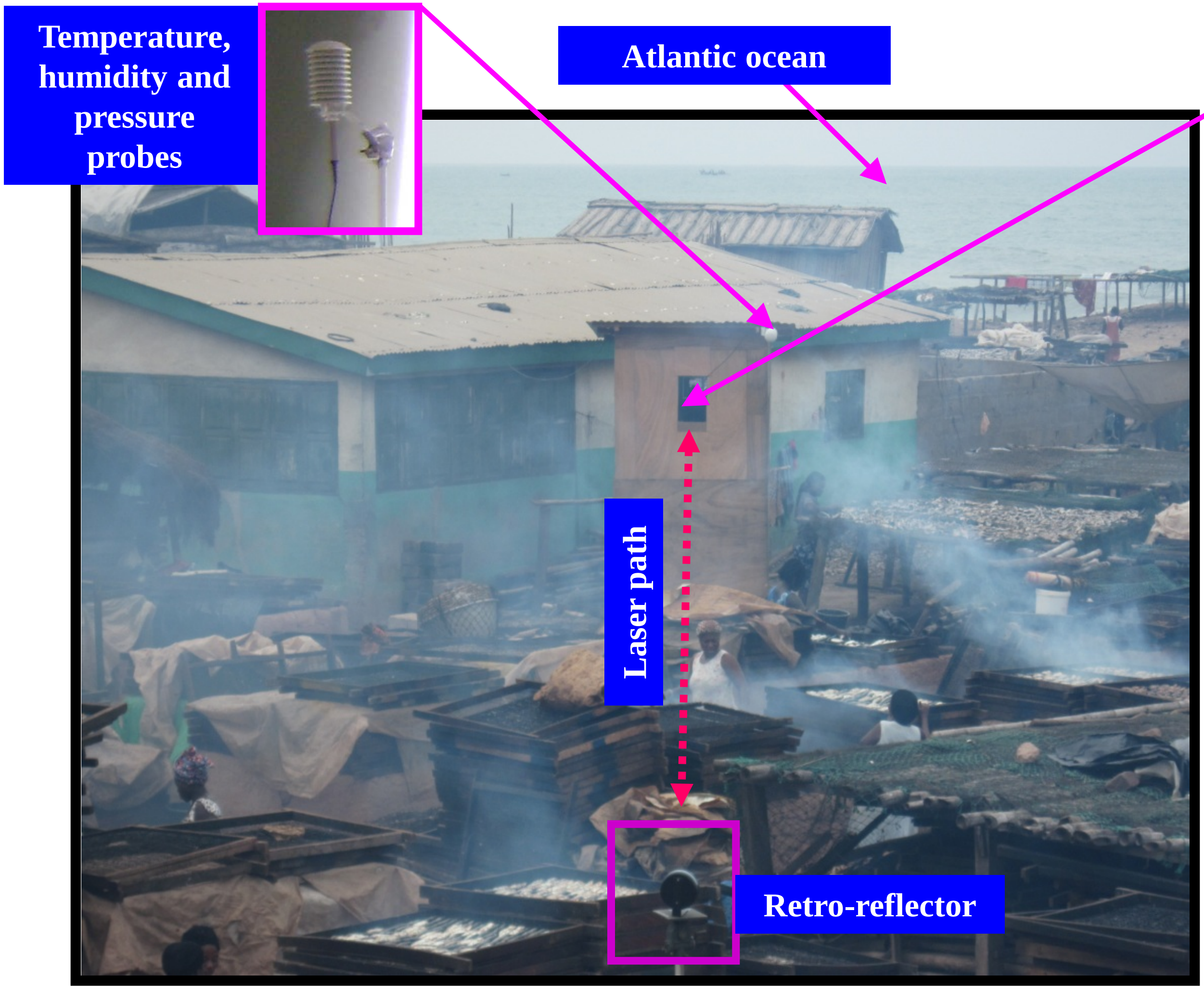

2010 Wood / Smoke Analysis

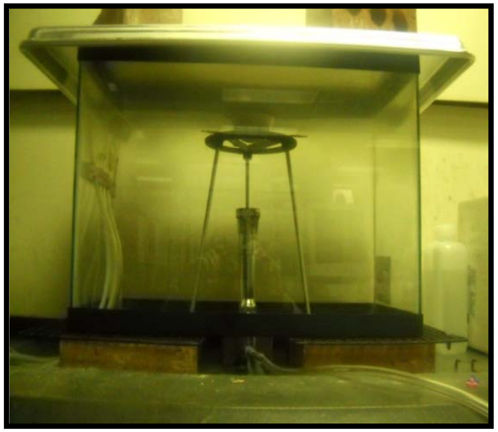

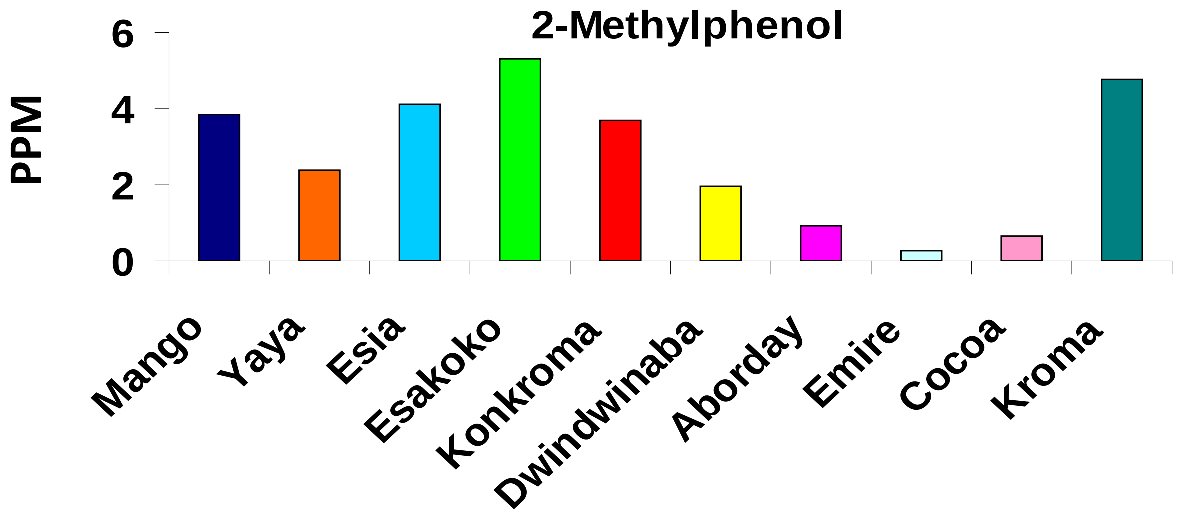

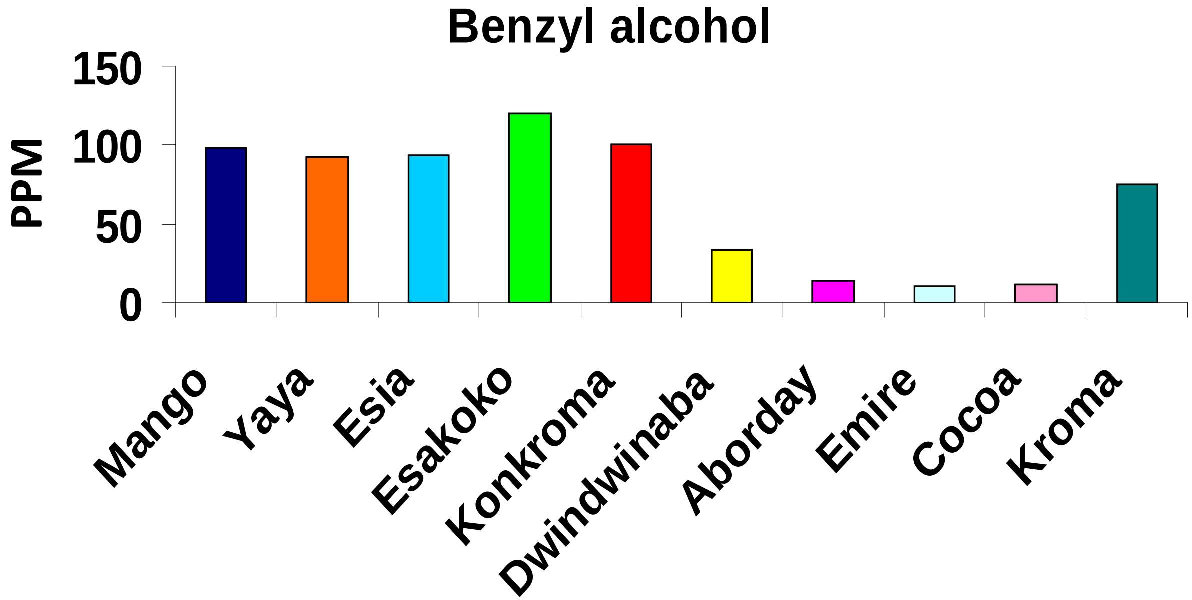

2010 Field Work – Results, …

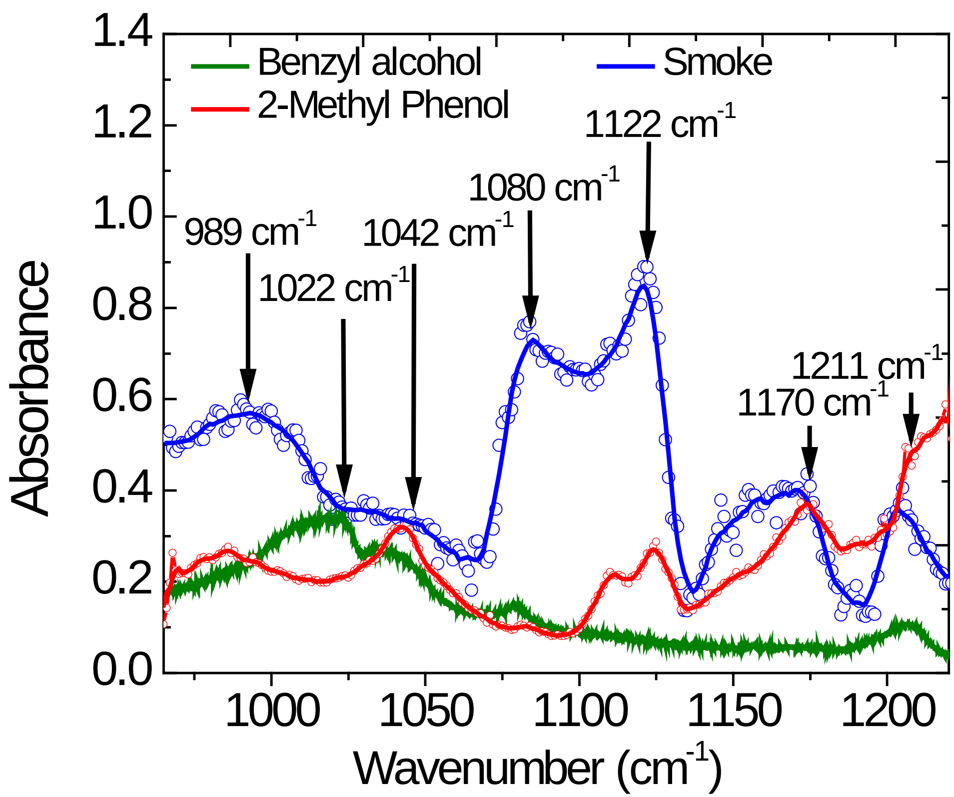

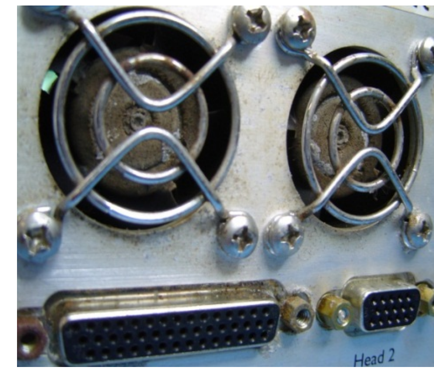

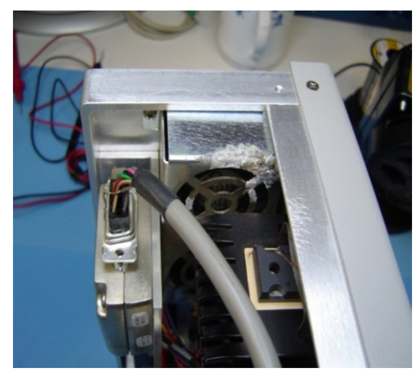

A Multi-Sensor Field Deployment for Assessing Anthropogenic Influences on Carbon, Nitrogen and Water Cycling

Two field deployments:

Part I: October 24-November 2, 2011; part II: April 13-25, 2012

David Miller et al.

N_2O

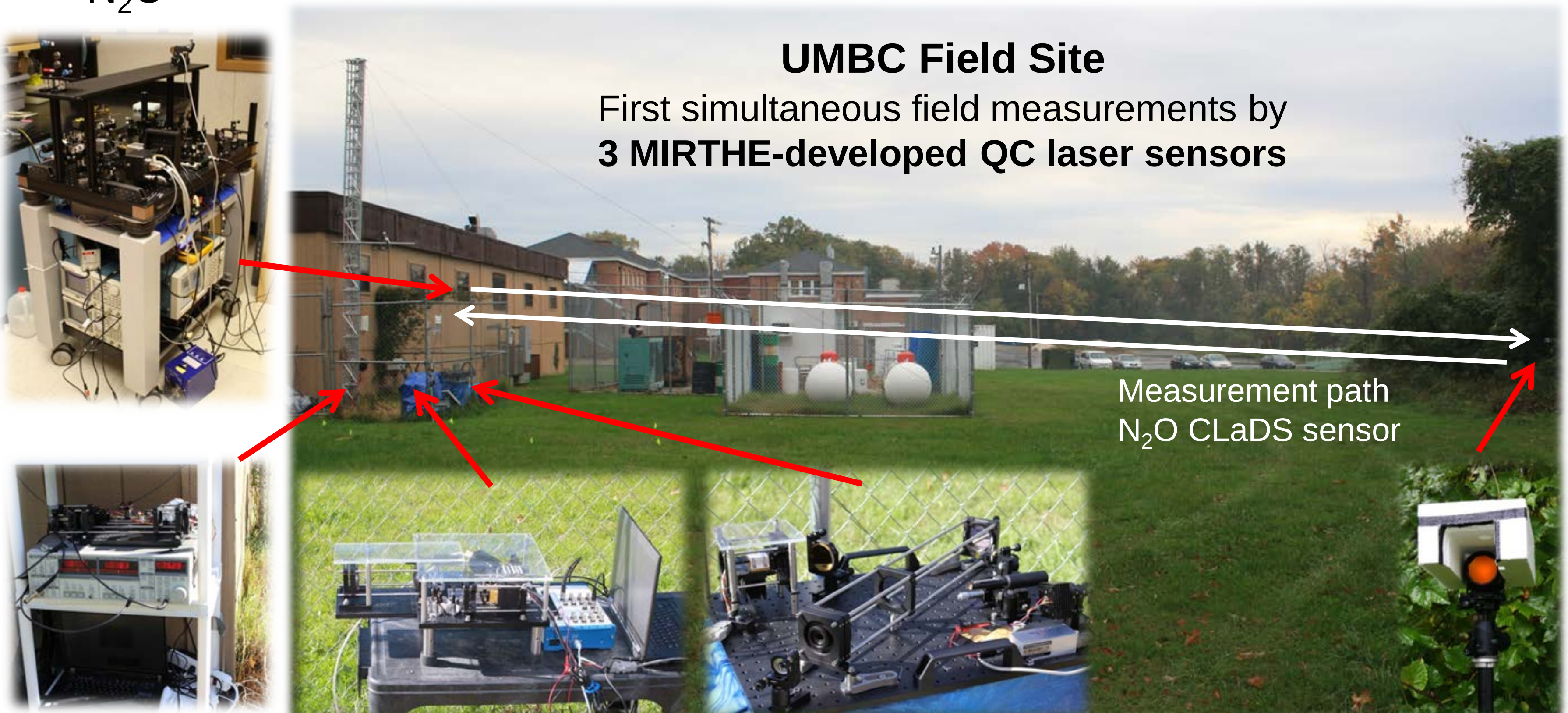

CO_2/CH_4 N_2O/CO NH_3 Retro-reflector

Collaborations:

Prof. Claire Welty, Chemical, Biochemical, and Environmental Engineering, UMBC and Baltimore Ecosystem Study

Ammonia in Breath

Prof. Frank Tittel, Rice U.
Dr. Steve Solga, M.D., St. Luke’s

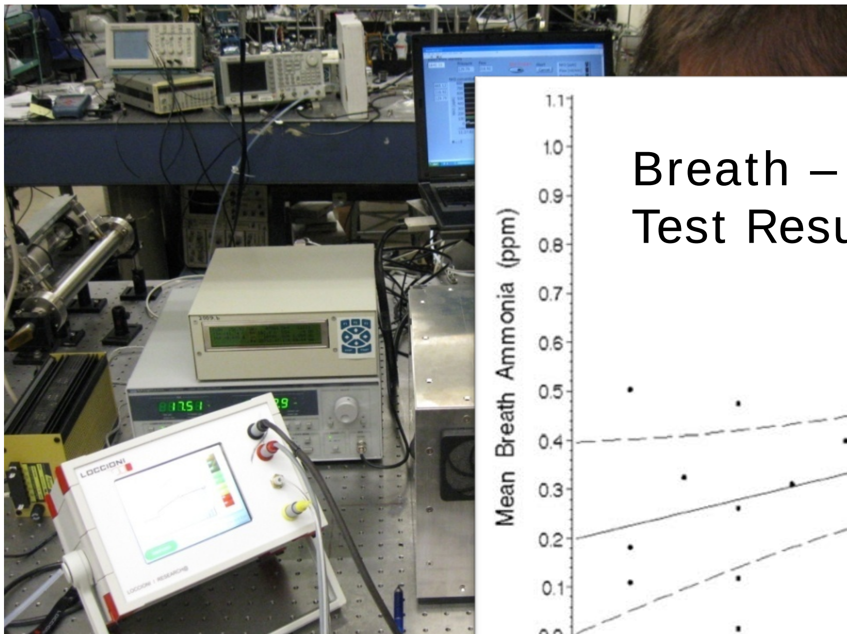

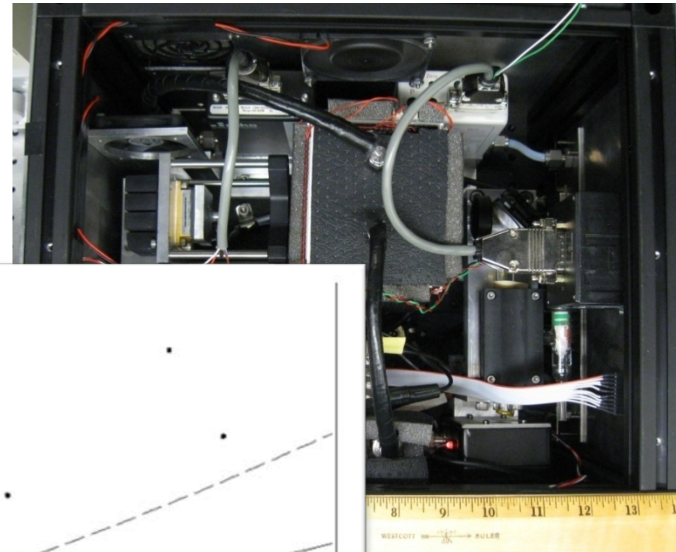

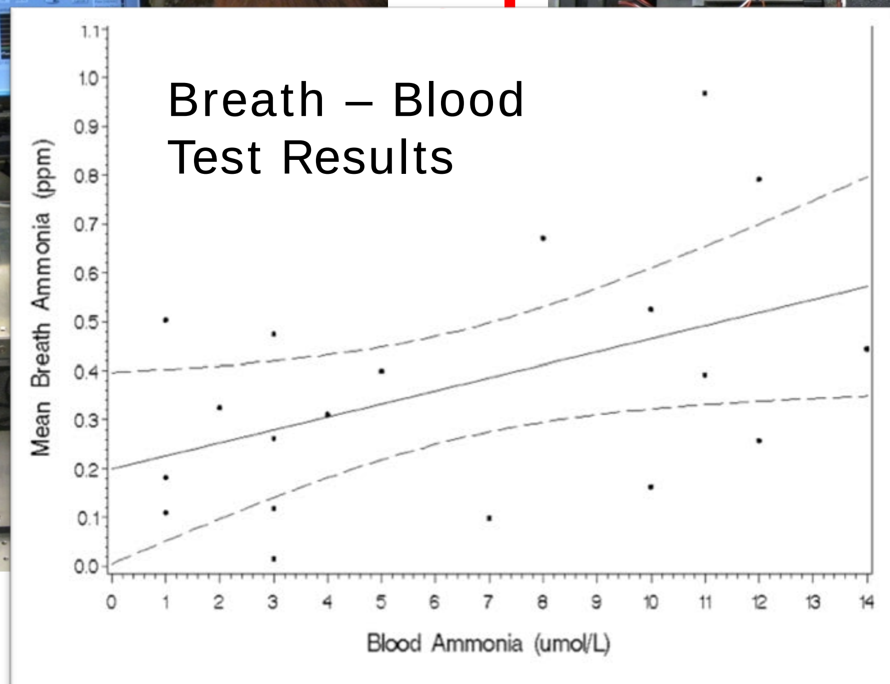

d in a 14” x 10” x 12” box.

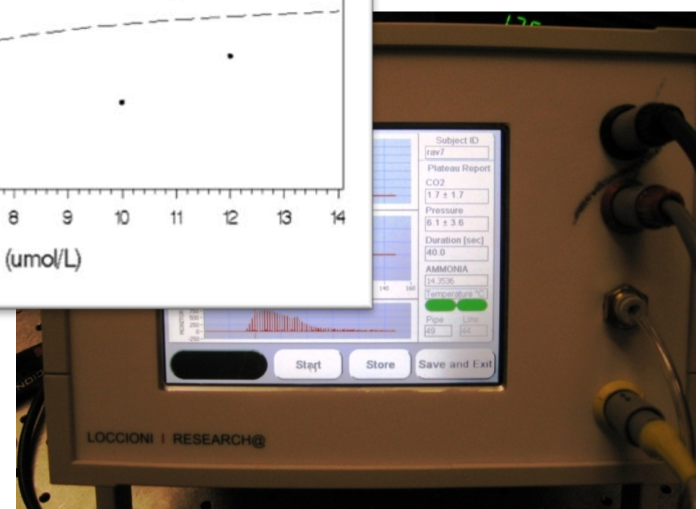

Breath analyzer from Loccioni

Non-Invasive Glucose Detection

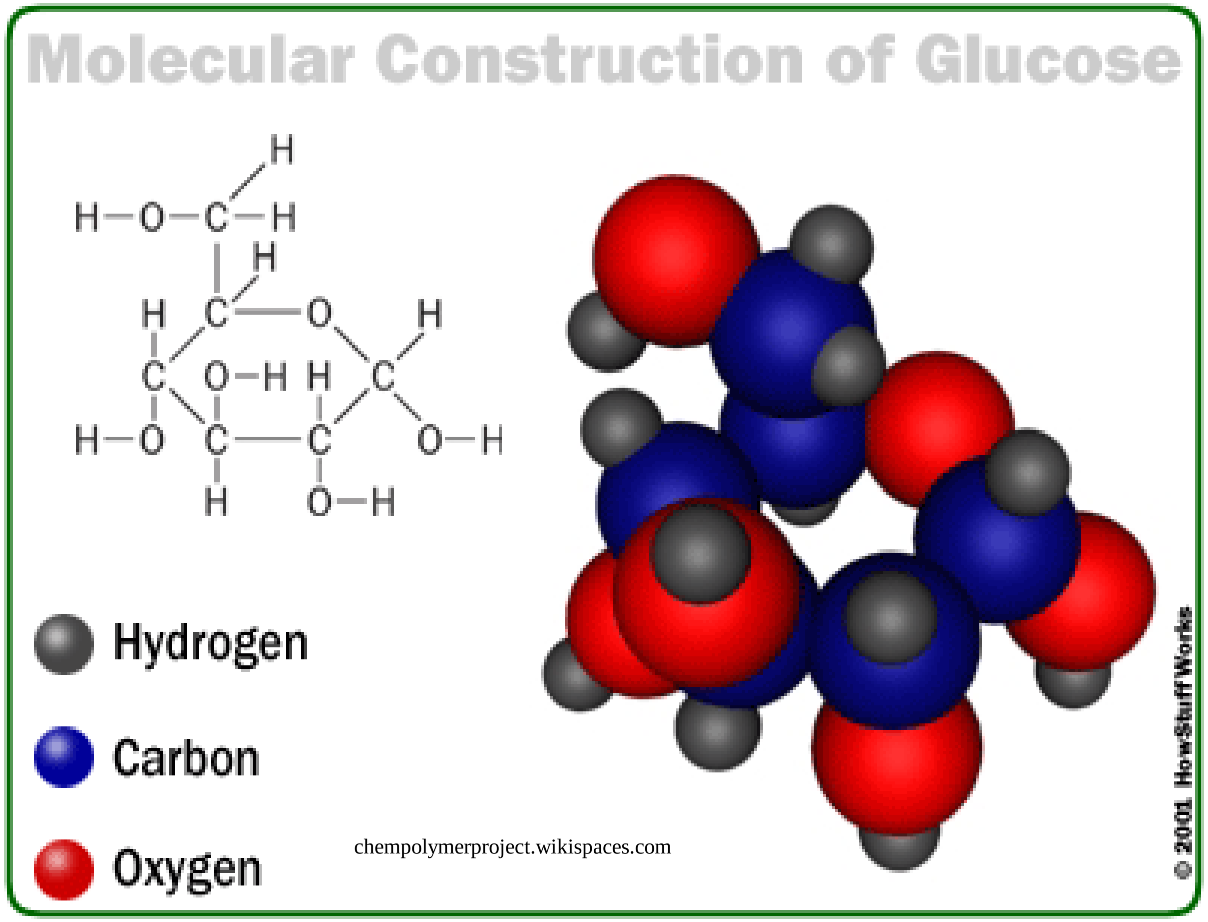

chempolymerproject.wikispaces.com

Scatterers in Skin

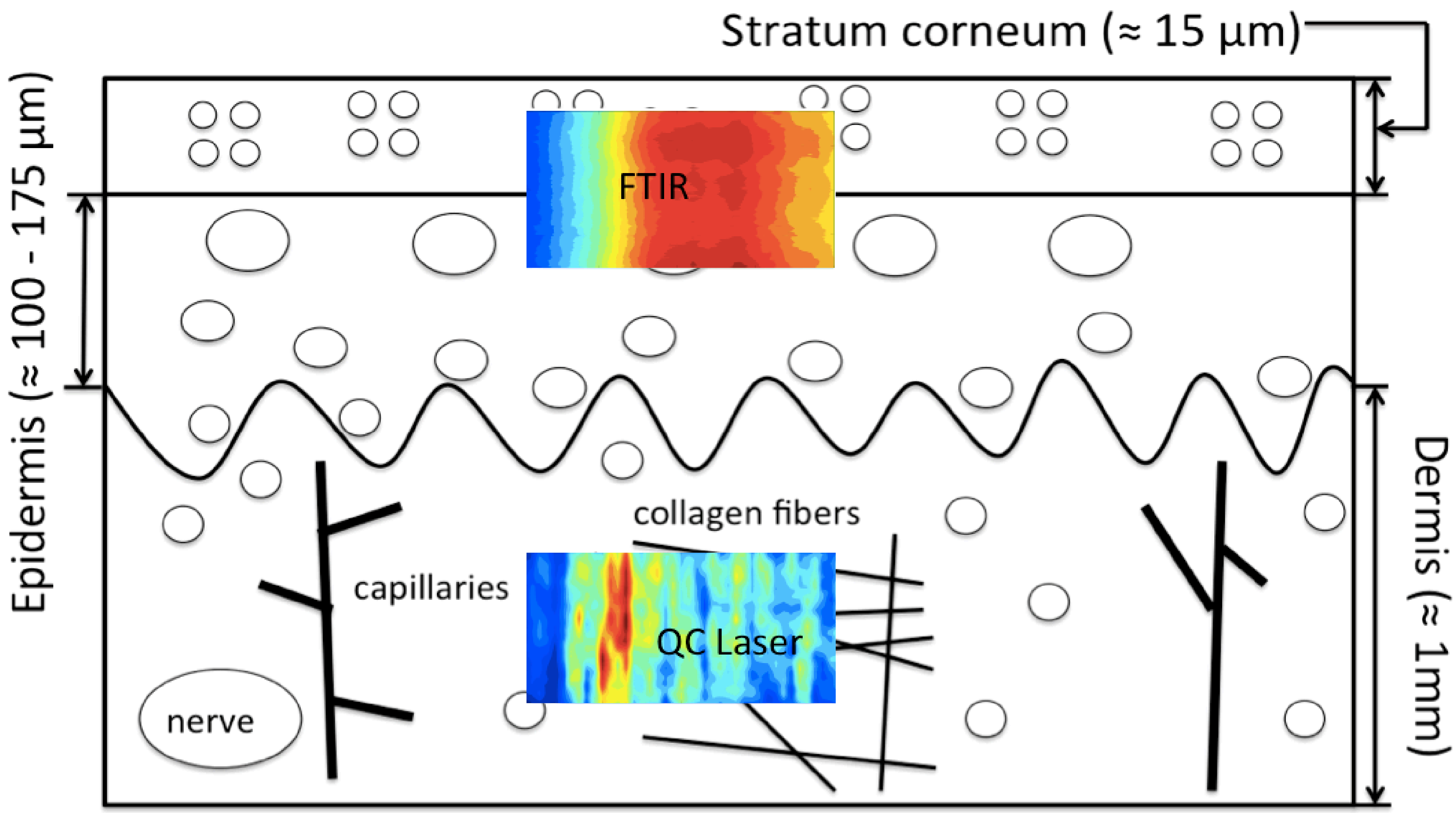

S. Liakat et al.

Acknowledgements

Students & post-docs & staff:

Nyan Aung
Ekua Bentil → Goldman Sachs
Pierre Bouzi
Richard Cendejas → Start-up in LA, CA
YenTing Chiu
Afusat Dirisu → NASA Goddard, AFOSR
Matt Escarra → Caltech, Tulane University
Kale Franz → NASA JPL , start-up
Anthony Hoffman → Princeton, Notre Dame
Scott S. Howard → Cornell, Notre Dame
Xue Huang
Loan T. Le
Sabbir Liakat
Peter Qiang Liu → ETH
Zhijun Liu → Brown, UCLA
Arvind Ravikumar
Arash Sadeghi
Yu Song
Akil Word-Daniels
Yu Yao → Harvard
Mei Chai Zheng

William Charles → start-up
Jianxin Chen → CAS Shanghai
Anna P. Michel → WHOI
Dan Wasserman → UML, UIUC

Germano Maioli Penello, Brazil
Elvis Mujagic, Austria
Kamil Sladek, Germany
+ summer students …

Growth:

U. Maryland Baltimore County:
Fow-Sen Choa & group
Maxion Technologies:
Fred Towner
AdTech Optics:
Xiaojun Wang & group
Corning Inc.:
Catherine G. Caneau, Chung-en Zah
The City College of New York:
Maria C. Tamargo

Theory:

Jacob Khurgin & group Johns Hopkins U.
Alexey Belyanin & group Texas A&M U.

Funding:

NSF, DARPA, NASA-JPL, Princeton U., …

Summer 2012